Influence of loading and cracks on carbonation of RC elements made of different concrete types

Wang, Xiao Hui; Val, Dimitri V.; Zheng, Li; Jones, M. Roderick

Published in:
Construction and Building Materials

DOI:
10.1016/j.conbuildmat.2017.12.142

Publication date:
2018

Influence of loading and cracks on carbonation of RC elements made of different concrete types

Xiao-Hui Wang[a], Dimitri V. Val[a], Li Zheng[b], M. Roderick Jones[b]

[a] Institute for Infrastructure & Environment, Heriot-Watt University, Edinburgh, UK

[b] Concrete Technology Unit, Division of Civil Engineering, University of Dundee, Dundee, UK

Abstract

Accurate prediction of the carbonation rate of a particular concrete is important for the correct assessment of both durability and environmental impact of reinforced concrete (RC) structures. Applied loading and caused by it concrete cracking are major factors affecting the carbonation, which so far have received little attention of researchers, especially this concerns 'green' concretes, i.e. concretes in which Portland cement (PC) is partially replaced by supplementary cementitious materials such as fly ash (FA) and ground granulated blast-furnace slag (GGBS). The aim of this paper is to present laboratory data arising from experiments to study the influence of static loading and associated concrete cracking on the carbonation resistance of RC elements made of PC concretes and 'green' concretes containing significant amounts FA and GGBS. For this purpose, six different concrete mixes with two different water/binder (w/b) ratios (0.40 and 0.55) and different proportions of PC, FA and GGBS were prepared. Twelve RC beams (100×120×900-mm) and a number of 100-mm concrete cubes were cast, 28-day cured and then kept for three months under temperature and relative humidity to reach equilibrium with those of an carbonation-accelerated chamber used in the tests. The RC beam specimens were loaded in four-point bending to produce tensile cracks of different widths and then placed into the carbonation chamber along with unloaded cube specimens to be subjected to accelerated carbonation for 120 days. Results of the experiments show a significant effect of loading (both tensile and compressive stresses) on the carbonation resistance of the concretes, especially of 'green' concretes.

Keywords: accelerated carbonation; Portland cement concrete; fly ash; granulated blast-furnace slag; loading; cracks.

1. Introduction

Climate change is one of the key challenges facing the human race in the 21st century. This phenomenon is primarily attributed to anthropogenic emissions of greenhouse gases, most notably carbon dioxide (CO_2). One of major global contributors to the anthropogenic CO_2 emissions is the concrete industry, which contributes 5% to those, mainly from a calcination reaction involved in the Portland cement production [Pade and Guimaraes 2007]. CO_2 emissions associated with the concrete industry can be reduced by decreasing the amount of Portland cement used in concrete. This is usually achieved by replacing Portland cement with supplementary cementitious materials (SCM), mostly industrial by-products such as fly ash, blast furnace slag and silica fume [eg Meyer 2009] or fillers such as limestone. Concretes containing such materials are often referred to as 'green' concretes [Damtoft et al. 2008]. A number of studies comparing the environmental impact of traditional and 'green' concretes have been published, (e.g. [Van den Heede and De Belle 2012, Van den Heede and De Belle 2014]).

After a concrete structure has been constructed the cement paste in the structure becomes exposed to carbon dioxide. During this process, CO_2 present in the atmosphere diffuses through air-filled pores in the concrete and reacts with the alkaline cement hydration products, in particular with calcium hydroxide, $Ca(OH)_2$. On one hand, carbonation has a positive environmental effect because CO_2 reabsorbed in this process partially offsets its emission during calcination [Haselbach 2009]. On the other hand, the reaction between CO_2 and $Ca(OH)_2$ reduces the alkalinity of the concrete pore solution and can lead to corrosion of reinforcing steel when the carbonation front reaches the steel (e.g. [Bentur et al. 1998]). This effect of carbonation on the durability of RC structures instigated research of this phenomenon, including experimental studies (e.g. [Ho and Lewis 1987, Sanjuan et al. 2003, Khunthongkeaw et al. 2006, Cui et al. 2015]), field measurements (e.g. [Parrot and Killoh 1989, Castro et al. 2000, Guiglia and Taliano 2013, Neves et al. 2013]) and modelling (e.g. [Papadakis et al. 1991, Saetta et al. 1993, Steffens et al. 2002, Bary and Sellier 2004, Burkan Isgor and Ghani Razaqpur 2004]). In particular, it has been observed that 'green' concretes containing SCM, particularly where Portland cement is directly replaced, can have lower resistance to carbonation than traditional ones (e.g. [Papadakis 2000, Khunthongkeaw et al. 2006, Lye et

al. 2015, Lye et al. 2016]). More recently, the positive effect of carbonation on the CO_2 balance of the concrete industry has also attracted attention of researchers (e.g. [Wu et al. 2014, Yang et al. 2014, Ashraf 2016]).

Since natural carbonation (i.e. carbonation under actual atmospheric conditions at which the CO_2 concentration is about 0.04%) is a very slow process, in order to obtain meaningful experimental results within a reasonable time accelerated carbonation tests with increased CO_2 concentrations are usually performed. The range of the CO_2 concentration used in such tests has varied between 1% and 100%, while in most of the tests it has been between 3% and 10% [Ashraf 2016]. Since an increase in the CO_2 concentration can affect chemical reactions and transport mechanisms involved in carbonation there has been an extensive discussion about the validity of the accelerated tests (e.g. [Sanjuan et al. 2003, Castellote et al. 2009, Visser 2014, Cui et al. 2015]). Although full consensus has not been reached, it has been recommended to keep the partial pressure of CO_2 between 3%-5%, in order to obtain results similar to natural conditions; in particular, this has been shown for 'green' concretes containing fly ash and blast furnace slag [Lye et al. 2015, Lye et al. 2016]. Among the factors which affect the rate of carbonation, loading and associated cracking have received limited attention and most research has been restricted to Portland cement concretes and effects of tensile stresses caused by static and cyclic loading [Castel et al. 1999, Alahmad et al. 2009, Jiang et al. 2015]. These studies have demonstrated that tensile stresses/strains have a major effect on carbonation of the elements, i.e. the carbonation rate is noticeably increased depending on the stress/strain level [Castel et al. 1999, Jiang et al. 2015]. It has also been shown that CO_2 can freely diffused through cracks >60 μm so that the carbonation depths perpendicular to the crack wall were similar to that at the concrete surface, the diffusion slowed down for smaller crack widths and there was no carbonation penetration perpendicular to the crack wall for crack widths of <9 μm [Alahmad et al. 2009]. It is worth to note that the CO_2 concentration used in this study was 50%.

Thus, the aim of th study described in this paper was to experimentally investigate the influence of static loading and associated cracking on the carbonation performance of RC elements made of Portland cement (PC) concretes and 'green' concretes containing fly ash (FA) and ground granulated blast-furnace

(GGBS). In this research, six different concrete mixes with two different water/binder (w/b) ratios (0.40 and 0.55) and different proportions of PC, FA and GGBS were prepared. The mixes were used to cast twelve RC beams (100×120×900-mm) and 100-mm concrete cubes. In order to reach equilibrium with the test conditions the specimens were stored for 3 months in the same temperature and relative humidity (RH) conditions to those of the carbonation chamber. The RC beam specimens were then loaded in four-point bending to produce cracks of different widths. After that both RC beam specimens (loaded) and concrete cubes (unloaded) were transferred to the carbonation chamber. The specimens were subject to accelerated carbonation for 120 days and the carbonation depths then measured. In the following, the experiments will be described in more detail and their results presented and discussed. Special attention will be paid to effects on carbonation of both tensile and compressive stresses, concrete cracking and casting position.

2. Experimental Programme

2.1 Materials

Six concrete mixes were used in this experimental study. All mixes included PC (CEM I 52.5 N), in two of them this cement was partially replaced by FA (30%) and in other two by GGBS (50%). The aggregates in all mixes were Cambusmore sand and 10-mm gravel. Half of the mixes had the w/b ratio of 0.55 and the other half of 0.40; a plasticizer was added to the mixes with the lower w/b ratio. Table 1 shows the mix constituent proportions per cubic metre of concrete and was provided by the precaster, who produced the test specimens prior to transfer to the laboratory. 8 mm and 10 mm reinforcing bars were used with yield strength of 500 MPa.

2.2 Test specimens

Twelve RC beams with a rectangular cross section of 100×120 mm and length 900 mm were cast. The beams were reinforced in the longitudinal direction with two 10-mm diameter deformed bars at the bottom (tensile reinforcement) and two 8-mm diameter plain bars at the top (compression reinforcement), and in the transverse direction with stirrups made of 8-mm diameter plain bars. The concrete cover of the longitudinal tensile bars was to be 25 mm. The spacing between the stirrups was 46 mm near the beam ends and 105 mm closer to the midspan, while the central 200-mm long part of the beams was without shear

reinforcement. Two vertical (i.e. along the beam depth) 18-mm diameter holes at 100 mm from the beam ends (so that the distance between the holes was 700 mm) were made in each beam in order to later create a four-point bending system. Figure 1 shows the beam dimensions and reinforcement details. The beams were cast horizontally in wood moulds as shown in Figure 2. In addition, to the beams, seven 100-mm cubes were cast from each mix to determine the compressive strength and porosity of concretes made of the mixes and also the carbonation rate of unloaded specimens. All specimens were standard cured for 28 days.

As noted previously, the specimens were fabricated by a precaster. Thus, compared to the fabrication of specimens in a laboratory, the composition and quality of the specimens were not fully controlled by the researchers. However, the tests were probably more realistic since the specimens were more representative of typical RC elements produced by the industry.

2.3 Preconditioning of the specimens

All specimens (i.e. both beams and cubes) intended for accelerated carbonation were kept for 3 months under ambient conditions (i.e. temperature and RH) similar to those in the carbonation chamber. The beam specimens were then quasi-statically loaded in four-point bending using a universal testing machine, as shown in Figure 3. In accordance to the beam dimensions (Figure 1), the distance between two supporting pins was 700 mm (i.e. they were placed at the location of the holes) and the distance between two loading pins 200 mm. The level of the applied load was controlled to ensure that the maximum width of cracks in the tensile zone of the beams due to bending was either 0.1 mm or 0.3 mm. The load required to induce 0.1-mm wide cracks was about two-thirds of that used to induce 0.3-mm wide cracks. At the same time three concrete cubes from each mix were tested to determine the compressive strength of the concretes. After the beams had been loaded and cracked, they were removed from the testing machine and placed in pairs back-to-back to create four-point bending again, like in the initial loading state. This time two pins of 25-mm in diameter were placed at a distance of 200 mm from each other between two beams in each pair (at the previous locations of the loading pins), while two 16-mm diameter steel bars were put through the holes in the beams and tightened until the cracks in the beams opened to approximately the same widths as previously in the testing machine.

The pre-tensioned bars were then locked in place (Figure 4(a)) and the beam pairs along with the cubes were placed into the carbonation chamber (Figure 4(b)).

The actual dimensions of the beams and cracks in each beam had been measured and recorded before the beams were put into the carbonation chamber (see Table 2). The beam designation identifies the concrete mix followed by two digits that defines the maximum width of the initial bending cracks (e.g. '040PC01' is a PC concrete beam with a w/b ratio of 0.40 and the maximum initial crack width of 0.1 mm). It should be noted that the beams were placed in pairs based on the concrete properties and not on the initial crack widths, i.e. all pairs except of one consisted of beams made from the same concrete type, e.g. 040PC01 and 040PC03, 055PC01 and 055PC03, etc. The only exception was a pair consisting of 040FA03(2) and 040GGBS03 (the second beam made from the 040GGBS concrete was not properly fabricated and had to be replaced by a spare beam from 040FA). This led to noticeable differences between the maximum crack widths measured after the beams were coupled in pairs (Table 2) and the maximum initial crack widths of 0.1 mm and 0.3 mm obtained in the testing machine.

2.4 Accelerated carbonation test and carbonation depth measurements

The beam specimens and the concrete cubes were kept in the carbonation chamber for 120 days. The chamber conditions were as follows: T=20±5ºC, RH=60±5% and CO_2 content of 4±0.50 %. The specimens were not removed from the chamber for the whole duration of the test so that the tensile forces in the pre-tensioned bars in the beam pairs could be partially lost over the time due to creep.

After the specimens had been removed from the carbonation chamber they needed to be split in halves to measure the carbonation depth. The central parts of the beams (about 500 mm long), which had been under load during the accelerated carbonation test, were cut along their length into five segments. The segments were then split or diamond sawn (if they contained stirrups) along their lengths. The split/sawn surfaces were sprayed with a phenolphthalein solution (see Figure 5) and the carbonation depths measured at 10 mm intervals. Additional measurements were taken at the locations where changes of the carbonation depth were observed (e.g. around cracks). The concrete cubes were tested in accordance to BS EN 12390-7:2009 to determine the absorption and void content of the concretes as shown in Table 3.

3. Test Results

3.1 Concrete properties

, As these mixes used direct replacement (Table 2), the 040PC concrete had the highest compressive strength and the 055FA – the lowest one. However, the GGBS concretes had compressive strengths close to those of the PC concretes and for the w/b ratio of 0.55 the compressive strength of the 055GGBS was higher than that of the 055PC. The latest result is in line with the values of the void content shown in Table 3. As has been shown by previous research, lower porosity typically corresponds to higher compressive strength [Kolias 1994; Chen et al 2013]. In fact, this trend can be observed for practically all values of the compressive strength and void content presented in Tables 2 and 3. The only exception is the 040GGBS concrete, which had slightly lower porosity than the 040PC concrete but also lower compressive strength. This was unexpected as the GGBS concretes had lower porosity than the PC mixes even though the reactions associated with GGBS has a slower rate compared to the hydration of PC. However, it is known that adding GGBS to PC concretes eventually leads to reduced porosity [Siddique and Iqbal Khan 2011]. Since the void content in the tests was measured in about 8 months after casting the specimens there was enough time to achieve this effect. It should also be noted that values of the compressive strength given in Table 2 were obtained after four months and not on 28 days. The older age of the concretes at the time of the compressive tests probably explains the small differences between the measured compressive strengths of the PC and GGBS concretes. It is worth to note that the main characteristic of concretes used in this study is the w/b ratio. This is in line with the fib Model Code 2010 [ ], in which the carbonation resistance of concretes is also primarily related to their w/b ratio.

3.2 Cracks in RC beam specimens

Cracks in the beam specimens were measured and recorded right before placing the specimens into the carbonation chamber. Three types of cracks were observed: (1) flexural cracks in the tensile zone at the bottom of the specimens; (2) shear cracks in the zones with shear stresses (i.e. zones within the loaded part of the beams outside the 200-mm central part); and (3) drying shrinkage cracks at the top of the beams (i.e.

near the casting surface). The recorded crack patterns on the lateral sides of the beam specimens are shown in Figures 6 – 8. For each beam specimen two crack patterns (i.e. on both lateral sides of the beam) were recorded and the records were distinguished as "L – R" and "R – L", i.e. from the left end of the beam to its right end and vice versa for the opposite side. Since most cracks extended through the whole beam width the patterns on the two lateral sides were usually quite similar and a typical format is given. The crack widths shown in the Figures were recorded at the bottom of the beams; their maximum values for each beam are also given in Table 2.

The specimens with the initial crack widths of 0.3 mm usually had wider cracks when loaded as the back-to-back pair than the ones with the initial 0.1-mm wide cracks. Moreover, the specimens with the initial 0.3-mm wide cracks also had noticeable shear cracks (e.g. 055PC03, 040FA03, 055FA03, etc.), while the ones with the initial 0.1-mm cracks either had none (e.g. 055PC01) or very few (e.g. 040FA01, 055FA01, etc.), see Figures 6 – 8. This can be explained by higher loads that had to be applied to the specimens in the universal testing machine to obtain wider flexural cracks. All specimens had drying shrinkage cracks near the top (casting) surface. However, in the specimens made from the PC concretes these cracks were shallow, while in the specimens made from the FA and GGBS concretes the shrinkage cracks were deeper and nearly connected with flexural cracks, so that the cracks practically extended through the whole beam depth (e.g. 040FA03, 055FA01, 040SG03, 055SG01).

As noted previously, the specimens were not removed from the carbonation chamber for the whole duration of the carbonation test (120 days) and loads in the pairs were not checked over that time. Thus, the loads could decrease due to creep and further shrinkage strains and the cracks partially close (compared to their dimensions shown in Figures 6 – 8) while the specimens were in the carbonation chamber.

3.3 Carbonation depths

As explained above, two types of specimens were used in the test: unloaded 100-mm concrete cubes and loaded RC beams. To measure carbonation depths in the cubes the latter were split in the middle into halves and the depths were measured for each half. The average carbonation depths at the top (cast surface) and bottom of the cubes are shown in Table 4. The influence of two-dimensional CO_2 penetration on the

carbonation depth is clearly visible near the corners of the specimens (see Figure 9). Thus, the carbonation penetrations near the corners were not taken into account in the calculations of the average carbonation depths. For all cubes the average carbonation depth at the top (i.e. near the cast surface) was larger than that at the bottom, which is typical and due to free water migration towards the as-cast surface.

The measured carbonation profiles for the beams are shown in Figures 10 – 12. They are shown for the same halves of the beams as the crack patterns in Figures 6 – 8. However, the crack patterns were recorded on the external lateral surfaces of the beams, while the carbonation depths were measured on the internal surfaces of the halves. Thus, an "R – L" carbonation profile corresponds to the "L – R" crack pattern with the same name and vice versa. In these Figures, the measured carbonation profiles are shown by black lines, vertical carbonation depths at crack locations (i.e. flexural cracks at the bottom and drying shrinkage cracks at the top) are indicated by red numbers and red straight lines with arrows at both ends, and horizontal carbonation penetration through the crack walls are indicated by blue numbers and blue straight lines with arrows at both ends. Some visible cracks are also shown by red lines.

Results of the measurements of the carbonation depths in the beam specimens are summarised in Table 4. The average carbonation depths were calculated based only on the measurements within the central 200-mm long parts of the beams, within which the bending stresses (i.e. tensile at the bottom and compressive at the top) were constant. This was done in order to exclude the influence of the stress magnitude on the carbonation depth for the same specimen, as noted in previous research [Castel et al. 1999]. Moreover, the influence of visible flexural cracks has also been excluded, i.e. the carbonation depths measured within the vicinity of visible flexural cracks have not been taken into account in the calculations of the average carbonation depths. The maximum carbonation depths given in Table 4 are based on all measurements for a particular specimen and usually coincide with the location of major cracks. The only exception was the 055FA01 specimen. As can be seen in Figure 11(c), the maximum carbonation depth (75.9 mm) was measured at the end of the central segment cut out from this specimen and there is a clear discontinuity in the carbonation depth between this segment and the adjacent one. This occurred due to the central segment being split unevenly along its length and the width of one of the 'halves' being smaller than the half-width of the beam.

Thus, the measured carbonation depth of 75.9 mm does not represent the carbonation penetration through the bottom surface of the beam (which is of interest) but is rather due to the carbonation penetration through the nearest lateral beam surface. Hence, the carbonation measurements near this end of the central segment have been excluded from the analysis of the test results.

Carbonation penetration for the 040PC03 specimen was observed only in a couple of isolated locations and thus was not included in the analysis.

4. Discussion

4.1 Influence of concrete type and water-binder ratio on carbonation resistance

The resistance of concretes to carbonation in the context of their properties depends mainly on their CO_2 binding capacity and degree of interconnected porosity (e.g. [Sisomphon and Franke 2007]). An increase in the w/b ratio increases the concrete porosity and, subsequently, decreases the concrete resistance to carbonation. Results of the tests for the same concrete type (i.e. PC, FA or GGBS) follow this trend. As can be seen from Table 3, the porosity of concretes of the same type with the w/b ratio of 0.55 is larger than those with w/b=0.40 and the average carbonation depth in the cubes is correspondingly larger (see Table 4). The situation becomes more complicated when PC concretes are compared with concretes with SMC and concrete elements are subject to loading. The latter will be discussed in the next section.

Replacement of PC in concrete with SCM reduces the amount of carbonatable constituents and, subsequently, the CO_2 binding capacity of the concrete that should lead to an increase in the carbonation rate. Direct replacement mix designs usually result in higher porosity of the concrete, although, as noted previously, concretes containing GGBS may eventually have lower porosity than PC ones with the same w/b ratio. In these tests, the 040PC concrete demonstrated the highest carbonation resistance although its porosity was slightly higher than that of the 040GGBS concrete. However, this was different for the PC and GGBS concretes with the w/b ratio of 0.55 – where the PC concrete had higher porosity than the 055GGBS (see Table 3), while its carbonation resistance was lower (see the corresponding average carbonation depths for the cubes in Table 4). This data shows that the lower porosity had a more significant effect on the

carbonation resistance of the 055GGBS concrete than its reduced CO_2 binding capacity compared to the 055PC.

The 040FA concrete also had lower porosity that the 055PC and 055GGBS concretes (see Table 3) but its carbonation resistance was also lower . The 055FA concrete had the highest porosity and the lowest carbonation resistance in unloaded state (see Table 4).

Based on the average carbonation depths for the cubes (Table 4), the concretes considered in this study can be ranked in the following order in terms of their carbonation resistance in unloaded state (from lowest to highest): 055FA, 040FA, 055PC, 055GGBS, 040GGBS and 040PC. It is important to highlight that these mixes did not have equal strength and that the rank order is likely to different when based on comparative strength rather than w/b.

The results for the FA concretes showing their lower carbonation resistance compared to that of PC and GGBS concretes are in line with most of the previous studies [Lye et al. 2015, Lye et al. 2016]. There is less consensus regarding the relative carbonation resistance of GGBS and PC concretes. It is often suggested that the carbonation resistance of GGBS concretes is lower than that of PC concretes with a similar w/b ratio, especially when the GGBS content is greater than 20% [Lye et al. 2016]. However, according to several studies, concretes with 50% GGBS content have more or less the same carbonation resistance as PC concretes with a similar w/b ratio [Osborne 1992, Polder et al. 2014] or similar strength grade [Bamforth 2004, Bouzoubaa and Foo 2005]. The results of this study for GGBS and PC concretes (with w/b=0.55) in unloaded state support the latter observations.

4.2 Influence of loading on carbonation resistance

Since in this study both unloaded and loaded (in four-point bending) specimens were subject to accelerated carbonation testing this allows to assess the influence of both compressive and tensile stresses in concrete on its carbonation. First of all, it is worth to note that while in each tested concrete cube the average carbonation depth at the top was larger than that at the bottom (due to casting direction) the opposite was observed in the beam specimens although the casting position was the same, i.e. the top was the beams'

casting surface (see Table 4). This demonstrates that compressive and tensile stresses had more significant influence on the carbonation resistance than the casting direction.

The results in Table 4 also shows that tensile stresses led to a decrease in the carbonation resistance, since the average carbonation depth at the bottom of each beam specimen was larger than that of the corresponding concrete cube. This is in agreement with previously reported experimental results [Castel et al. 1999]. As can be seen, the largest increase in the average carbonation depth due to tensile stresses was observed in the beams made of the concretes with SCM and the w/b ratio of 0.55, i.e. 055FA (48.1 mm in 055FA01 and 38.8 mm in 055FA03 versus 18.5 mm in the corresponding cube) and 055GGBS (24.4 mm and 29.8 mm in the beams versus 12.0 mm in the cube). Regarding the beams made from 055FA, it is necessary to note that the results could be partially influenced by flexural cracks; in particular, for the 055FA01, in which the flexural cracks were spaced much closer (average spacing 60 mm – see Figure 7(c)) than in the other specimens (average spacing 90-95 mm – see Figures 6-8). Thus, it was difficult to distinguish between the vertical penetration of CO_2 through the bottom surface of the 055FA01 beam and the horizontal penetration through the crack walls. In the unloaded state, the 055GGBS concrete had a higher carbonation resistance than the 055PC and 040FA mixes due to its lower porosity than that of 055PC and higher CO_2 binding capacity than that of 040FA. Damage to the concrete (i.e. micro-cracking) caused by tensile stresses negated these advantages of the 055GGBS in the context of carbonation resistance - as can be seen from Table 4 the average carbonation depth at the bottom of the 055GGBS beams is larger than that at the bottom of the 055PC and 040FA beams. As in the unloaded state, under tensile stresses the 055FA concrete had the lowest carbonation resistance among all considered concretes. According to the average carbonation depths at the bottom of the beam specimens shown in Table 4, the concretes can be ranked in the following order in terms of their carbonation resistance under tensile stresses (from lowest to highest): 055FA, 055GGBS, 040FA, 055PC, 040GGBS and 040PC. Again, it is important to note the caveat that this is not based on equal strength.

While in the past the main attention has been on the influence of tensile stresses on the carbonation resistance of concrete (e.g. [Castel et al. 1999, Jiang et al. 2015]) in this research the influence of

compressive stresses has also been studied . Based on the average carbonation depths measured at the top (i.e. in compression zone) of the beam specimens (Table 4), compressive stresses have a positive effect on the carbonation resistance of concrete. One possibility to explain this is that compressive stress closes microcracking and hence reduces the degree of interconnected voidage but since this could only be measured on unloaded specimens it was not possible to confirm this hypothesis. Only in three beam specimens: 055FA01, 055GGBS01 and 055GGBS03, the average carbonation depth at the top was larger than that at top of the corresponding concrete cubes. However, the presence of comparatively large drying shrinkage cracks in these three beams (see Figures 7(c), 8(b) and (c)) potentially negated the effect of compressive stresses on microcracks. Based on the average carbonation depths for the beams made from the same mix type, the concretes can be ranked in the following order in terms of their carbonation resistance under compressive stresses (from lowest to highest): 055FA, 055GGBS, 040FA, 055PC, 040GGBS and 040PC, which is the same that noted for the tensile stressed concrete.

Thus, comparing the results for the loaded and unloaded states it can be concluded that the 055GGBS concrete has been more negatively affected by loading, in terms of the carbonation resistance, than the 055PC and 040FA concretes.. The positive effect of GGBS on the concrete porosity (and, subsequently, on the carbonation resistance) was negated by micro-cracks due to tensile stresses in the tension zone and drying shrinkage cracks in the compression zone. The other concrete, where carbonation resistance was significantly affected by loading, was the 055FA (see Table 4). However, this mix demonstrated the lowest carbonation resistance in both loaded and unloaded states.

4.3 Influence of cracking and other factors on carbonation resistance

As noted previously, three types of cracks: flexural, shear and drying shrinkage, were observed in the beam specimens. The influence of flexural cracks on the vertical carbonation penetration (i.e. through the bottom surface of the beams) can be observed in all beam specimens – the maximum carbonation depths at the bottom of the beams, which are summarised in Table 4, coincide with the location of the flexural cracks. The only exception is the 055FA01 beam, in which the maximum carbonation depth (75.9 mm) according to the carbonation profile shown in Figure 11(c) is on the border between two segments. However, as

explained previously in Section 3.3, this result does not represent the CO_2 penetration through the bottom surface of the beam and should be excluded from consideration. The next largest value (64.1 mm), which is given in Table 4, is at the location of a flexural crack. There is also carbonation penetration perpendicular to the crack walls, which according to previous research depends on the crack width. In particular, it was observed that in cracks of 0.06-mm wide or wider the depth of this penetration was similar to that at the concrete surface [Alahmad et al. 2009]. The CO_2 penetration perpendicular the walls of the flexural cracks can be clearly seen in a number of the carbonation profiles measured in the present study, e.g. 055PC01 (Figure 10(a)), 040FA01 (Figure 11(a)), 040FA03(2) (Figure 11(b)), 040GGBS03 (Figure 12(a)) and 055GGBS03 (Figure 12(c)). At the same time, it can also be seen that no (or almost no) CO_2 penetration perpendicular to the crack wall was observed for many flexural cracks appearing in the crack patterns (Figures 6-8). As noted previously, the crack patterns had been recorded before the beams were placed into the carbonation chamber. Since loads applied to the beams were not controlled while the beams were in the carbonation chamber the loads could decrease due to concrete creep and the compression cracks could partially (or fully) close. Alahmad et al. [2009] noted that there was no CO_2 penetration perpendicular to the crack wall was observed for cracks narrower than 0.01 mm; however, the CO_2 concentration used in their tests was 50%. Thus, it can be expected that in the present tests with the CO_2 concentration of 4% no noticeable CO_2 penetration perpendicular to the crack wall was observed even for slightly wider cracks. The 055FA01 beam is a special case – as the spacing between flexural cracks in this beam was smaller than in the other beams (on average 60 mm versus 90-95 mm in the others) so that areas between the flexural cracks could be fully carbonated due to CO_2 penetration through the crack walls that creates an impression of more or less uniform vertical propagation (i.e. from the bottom of the beam upwards) of the carbonation front (see Figure 11(c)).

Shear cracks were observed in the beam specimens that were initially loaded to create 0.3 mm flexural cracks. Among these specimens, the CO_2 penetration perpendicular to the shear crack walls can be seen in 055PC03, 055FA03 and 055GGBS03 (Figures 10(b), 11(d) and 12(c), respectively). Larger opening of the shear cracks in these specimens that caused this penetration can be explained by lower strength of the

specimens' concretes compared to the corresponding 0.40 w/b specimens.

Drying shrinkage cracks had a smaller effect on the carbonation propagation compared to the flexural cracks, e.g. the maximum carbonation depths at the top (see Table 4) rarely coincide with the location of drying shrinkage cracks (see Figures 10-12). This is probably due to compressive stresses reducing the crack widths. In fact, in most specimens the average carbonation depth at the top (that was calculated taking into account all carbonation measurements there) is less than that in the corresponding unloaded cubes (see Table 4), which did not have drying shrinkage cracks. The exception are the beams made from the 055GGBS concrete – in these two beams the average carbonation depths at the top are larger than in the corresponding cube that can be attributed to influence of the drying shrinkage cracks.

Another factor that influenced the carbonation of the beam specimens is the use of stirrups. It has been shown previously that carbonation occurs at the steel-concrete interface, where it intercepts a crack, irrespective of the crack width [Alahmad et al. 2009, Ghantous et al. 2017]. The same phenomenon was observed in these tests, e.g. larger carbonation depths under stirrups at the interception of drying shrinkage cracks (i.e. at the top of the beam) are clearly noticeable in, e.g., 050PC01 (Figure 10(a)), 050PC03 (Figure 10(b)), 055FA03 (Figure 11(d)) and 040GGBS03 (Figure 12(a)).

5. Conclusions

Accelerated carbonation tests of PC and 'green' (with FA and GGBS) concretes in unloaded and loaded states have been described. The emphasis of this research has been on studying the influence of loading, i.e. imposed stresses (both tensile and compressive), cracking and casting position on the carbonation of the concretes.

Based on the data generated the following conclusions can be made:

1) The concrete composition, including the w/b ratio, had a major influence on the carbonation resistance of the concretes. As expected, concretes of the same type with the larger w/b ratio of 0.55 had lower carbonation resistance than those with the w/b ratio of 0.40. Generally, replacing PC with FA and GGB led to a reduction of the carbonation resistance. The only exception is the 055GGBS concrete that had

higher carbonation resistance in the unloaded state than the 055PC concrete. The concretes with FA had lower carbonation resistance than those with PC and GGBS with the same w/b ratio. Based on equal w/b ratio the concretes can be ranked in the following order in terms of their carbonation resistance in the unloaded state (from lowest to highest): 055FA, 040FA, 055PC, 055GGBS, 040GGBS and 040PC.

2) The casting position had a noticeable influence on the carbonation resistance of the concretes in the unloaded state. In all unloaded specimens the carbonation depth at the top (i.e. casting surface) was lower than that at the bottom. This can be attributed to better concrete compaction at the bottom.

3) Loading had a major influence on the carbonation resistance of the concretes. Generally, compressive stresses led to an increase in the carbonation resistance of the concretes, while tensile stresses resulted in its decrease. The 055GGBS and 055FA concretes were mostly affected by loading in terms of their carbonation resistance. The concretes can be ranked in the following order in terms of their carbonation resistance under loading (from lowest to highest): 055FA, 055GGBS, 040FA, 055PC, 040GGBS and 040PC.

4) Flexural cracks clearly affected the upward propagation of the carbonation front. In all beam specimens the maximum carbonation depths at the bottom coincide with the location of the flexural cracks. The penetration of CO_2 perpendicular to the walls of flexural and shear cracks were also observed. In a number of the beam specimens the depths of this penetration were similar to those at the beam surface. Drying shrinkage cracks did not have such a noticeable effect on the carbonation propagation as flexural cracks. It can be attributed to the location of the drying shrinkage cracks in the compression zone of the beams so that compressive stresses caused the cracks' closure. The only exception is the beams made from the 055GGBS concrete, in which the average carbonation depth at the top was larger than that in the corresponding unloaded specimen. Thus, multiple drying shrinkage cracks in these beams negated the positive effect of compressive stresses so that the carbonation resistance of the concrete at the top decreased compared to the unloaded state.

Acknowledgments

This research was supported by the HORIZON 2020 Marie Skłodowska-Curie Research Fellowship Programme H2020 - 658475, titled: Climate-resilient pathways for the development of concrete infrastructure: adaptation, mitigation and sustainability (ClimatCon).

References

[1] C. Pade, M. Guimaraes, The CO_2 uptake of concrete in a 100 year perspective, Cem. Concr. Res. 37 (2007) 1348–1356.

[2] C. Meyer, The greening of the concrete industry, Cem. Concr. Compos. 31(8) (2009) 601-605.

[3] J.S. Damtoft, J. Lukasik, D. Herfort, D. Sorrentino, E.M. Gartner, Sustainable development and climate change initiatives, Cem. Concr. Res. 8 (2008) 115-127.

[4] P. Van den Heede, N. De Belie, Environmental impact and life cycle assessment (LCA) of traditional and 'green' concretes: Literature review and theoretical calculations, Cem. Concr. Compos. 34 (2012) 431-442.

[5] P. Van den Heede, N. De Belie, A service life based global warming potential for high-volume fly ash concrete exposed to carbonation, Constr. Build. Mater. 55(31) (2014) 183-193.

[6] L. Haselbach, Potential for carbon dioxide absorption in concrete, J. Environ. Eng. ASCE 135(6) (2009) 465-472.

[7] A. Bentur, N. Berke, S. Diamond, Steel Corrosion in Concrete: Fundamentals and Civil Engineering Practice, E&FN Spon Press, London, 1998.

[8] D.W.S. Ho, R.K. Lewis, Carbonation of concrete and its prediction, Cem. Conc. Res. 17(3) (1987) 489-504.

[9] M.A. Sanjuan, C. Andrade, M. Cheyrezy, Concrete carbonation tests in natural and accelerated conditions, Adv. Cem. Res. 15(4) (2003) 171-180.

[10] J. Khunthongkeaw, S. Tangtermsirikul, T. Leelawat, A study on carbonation depth prediction for fly ash concrete, Constr. Build. Mater. 20(9) (2006) 744-753.

[11] H. Cui, W. Tang, W. Liu, Z. Dong, F. Xing, Experimental study on effects of CO_2 concentrations on concrete carbonation and diffusion mechanisms, Constr. Build. Mater. 93 (2015) 522-527.

[12] L.J. Parrot, D. Killoh, Carbonation in a 36 year old in-situ concrete, Cem. Concr. Res. 19(4) (1989) 649-656.

[13] P. Castro, E.I. Moreno, J. Genesca, Influence of marine micro-climates on carbonation of reinforced concrete buildings, Cem. Concr. Res. 30 (2000) 1565-1571.

[14] M. Guiglia, M. Taliano, Comparison of carbonation depths measured on in-field exposed existing r.c. structures with predictions made using fib-Model Code 2010, Cem. Concr. Compos. 38 (2013) 92-108.

[15] R. Neves, F. Branko, J. de Brito, Field assessment of the relationship between natural and accelerated concrete carbonation resistance, Cem. Concr. Compos. 41 (2013) 9-15.

[16] V.G. Papadakis, C.G. Vayenas, M.N. Fardis, Fundamental modeling and experimental investigation of concrete carbonation, ACI Mater. J. 88 (1991) 363-373.

[17] A.V. Saetta, B.A. Schrefler, R.V. Vitaliani, The carbonation of concrete and the mechanisms of moisture, heat and carbon dioxide flow through porous materials, Cem. Concr. Res. 23(4) (1993) 761-772.

[18] A. Steffens, D. Dinkler, H. Ahrens, Modeling carbonation for corrosion risk prediction of concrete structures, Cem. Concr. Res. 32 (2002) 935-941.

[19] B. Bary, A. Sellier, Coupled moisture-carbon dioxide-calcium transfer model for carbonation of concrete, Cem. Concr. Res. 34 (2004) 1859-1872.

[20] O. Burkan Isgor, A. Ghani Razaqpur, Finite element modeling of coupled heat transfer, moisture transport and carbonation process in concrete structures, Cem. Concr. Compos. 26 (2004) 57-73.

[21] V.G. Papadakis, Effect of supplementary cementing materials on concrete resistance against carbonation and chloride ingress, Cem. Concr. Res. 30(2) (2000) 291-299.

[22] C.-Q. Lye, G.S. Ghataora, R.K. Dhir, Carbonation resistance of fly ash concrete, Mag. Concr. Res. 67(21) (2015) 1150-1178.

[23] C.-Q. Lye, G.S. Ghataora, R.K. Dhir, Carbonation resistance of GGBS concrete, Mag. Concr. Res. 68(18) (2016) 936-969.

[24] P. Wu, B. Xia, X. Zhao, The importance of use and end-of-life phases to the life cycle greenhouse gas (GHG) emissions of concrete – A review, Renew. Sustain. Energy Rev. 37 (2014) 360-369.

[25] K.-H. Yang, E.-A. Seo, S.-H. Tae, Carbonation and CO_2 uptake of concrete, Environ. Impact Assess. Rev. 46 (2014) 43–52.

[26] W. Ashraf, Carbonation of cement-based materials: Challenges and opportunities, Constr. Build. Mater. 120 (2016) 558-570.

[27] M. Castellote, L. Fernandez, C. Andrade, C. Alonso, Chemical changes and phase analysis of OPC pastes carbonated at different CO2 concentrations, Mater. Struct. 42 (2009) 515-525.

[28] J.H.M. Visser, Influence of the carbon dioxide concentration on the resistance to carbonation of concrete, Construct. Build. Mater. 67 (2014) 8-13.

[29] A. Castel, R. Francois, G. Arliguie, Effect of loading on carbonation penetration in reinforced concrete elements, Cem. Concr. Res. 29(4) (1999) 561-565.

[30] S. Alahmad, A. Toumi, J. Verdier, R. Francois, Effect of crack opening on carbon dioxide penetration in cracked mortar samples, Mater. Struct. 42 (2009) 559-566.

[31] C. Jiang, X. Gu, W. Zhang, W. Zou, Modeling of carbonation in tensile zone of plain concrete beams damaged by cyclic loading, Constr. Build. Mater. 77 (2015) 479-488.

[32] BS EN12390-7:2009, Testing hardened concrete, Part 7: Density of hardened concrete, 2009.

[33] S. Kolias, Investigation of the possibility of estimating concrete strength by porosity measurements. Mater. Struct. 27(5) (1994) 265–272.

[34] X. Chen, S. Wu, J. Zhou, Influence of porosity on compressive and tensile strength of cement mortar, { HYPERLINK "http://www.sciencedirect.com/science/journal/09500618" \o "Go to Construction and Building Materials on ScienceDirect" }. 40 (2013) 869-874.

[35] R. Siddique, M. Iqbal Khan, Supplementary Cementing Materials, Springer, Berlin, 2011.

[36] K. Sisomphon and L. Franke, Carbonation rates of concretes containing high volume of pozzolanic materials, Cem. Concr. Res. 37 (2007) 1647-1653.

[37] G.J. Osborne, Durability of Blastfurnace Slag Cement Concretes, Information Paper 6/92, BRE,

Bracknell, UK, 1992.

[38] R.B. Polder, T.G. Nijland, R. Mario, Blast Furnace Slag Cement Concrete in High Slag Content (CEM III/B), Report 270, Department of Traffic Safety, Environment and Technology, Delft, The Netherlands, 2014.

[39] P.B. Bamforth, Enhancing Reinforced Concrete Durability: Guidance on Selecting Measures for Minimising the Risk of Corrosion of Reinforcement in Concrete, Technical Report 61, BRE/Concrete Society, Bracknell, UK, 2004.

[40] N. Bouzoubaa, S. Foo, Use of Fly Ash and Slag in Concrete: A Best Practice Guide. Government of Canada Action Plan 2000 on Climate Change, Ottawa, ON, pp. 1-46, 2005.

[41] M.R. Ghantous, S. Poyet, V. L'Hostis, N.-C. Tran, R. Francois, Effect of accelerated carbonation conditions on the characterization of load-induced damage in reinforced concrete members, Mater. Struct. 50 (2017) 175.

List of figure captions

List of table captions

Figures

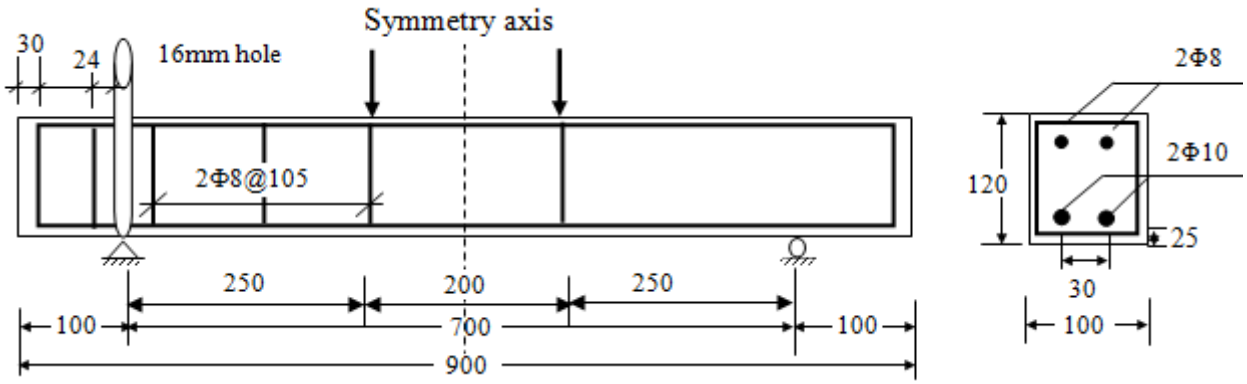

Figure 1. Sketch of RC beam specimen (all dimensions are mm).

Figure 2. Wood mold and casted beam specimens.

Figure 3. Setup for four-point bending.

(a)

(b)

Figure 4. Beam specimens in pairs: (a) connection; (b) in carbonation chamber.

(a)

(b)

(c)

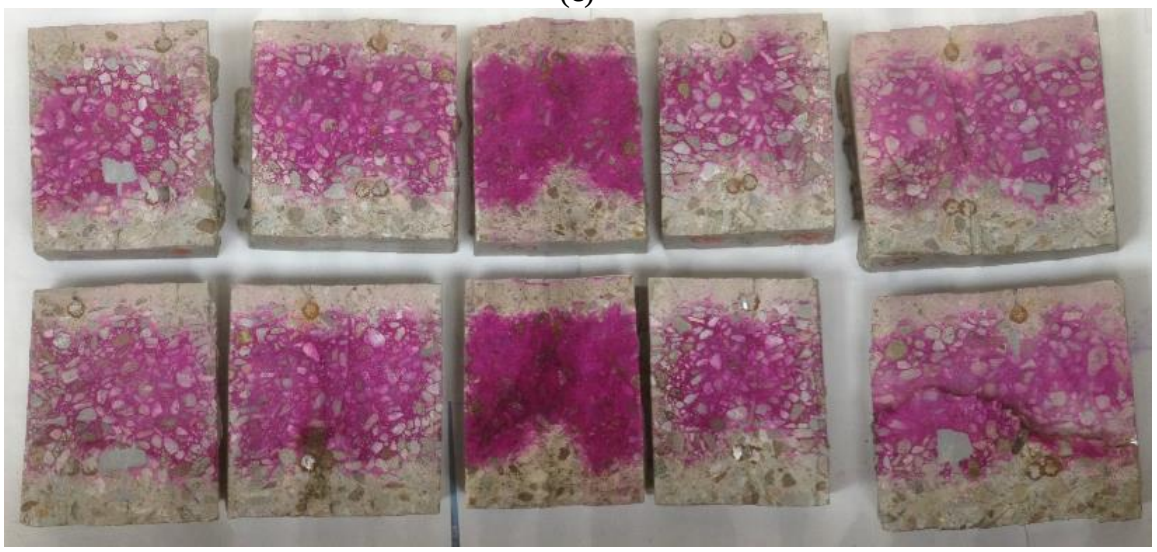

(d)

Figure 5. Preparing a beam specimen for carbonation measurements.

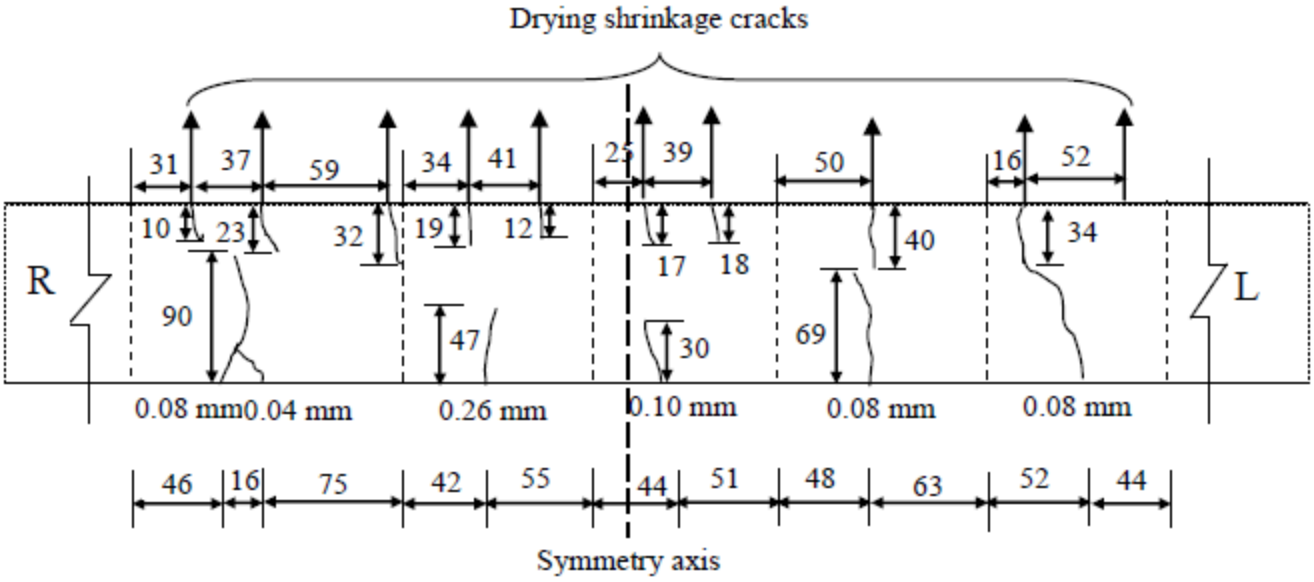

(a)

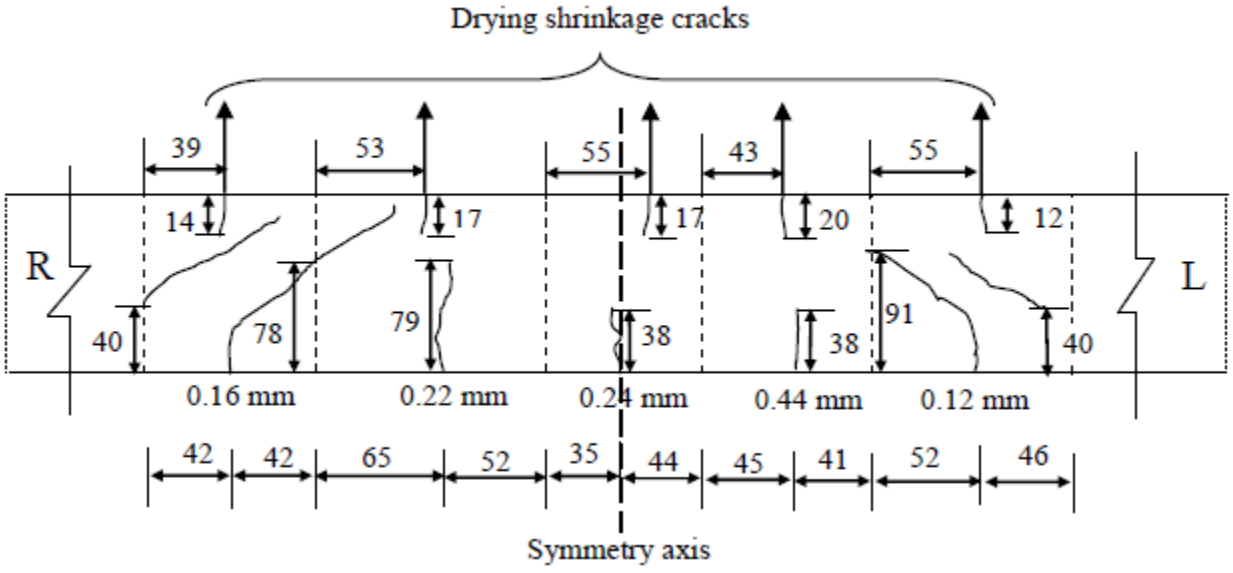

(b)

Figure 6. Crack patterns on lateral surfaces of the beam specimens made from 055PC concrete: (a) 055PC01; (b) 055PC03.

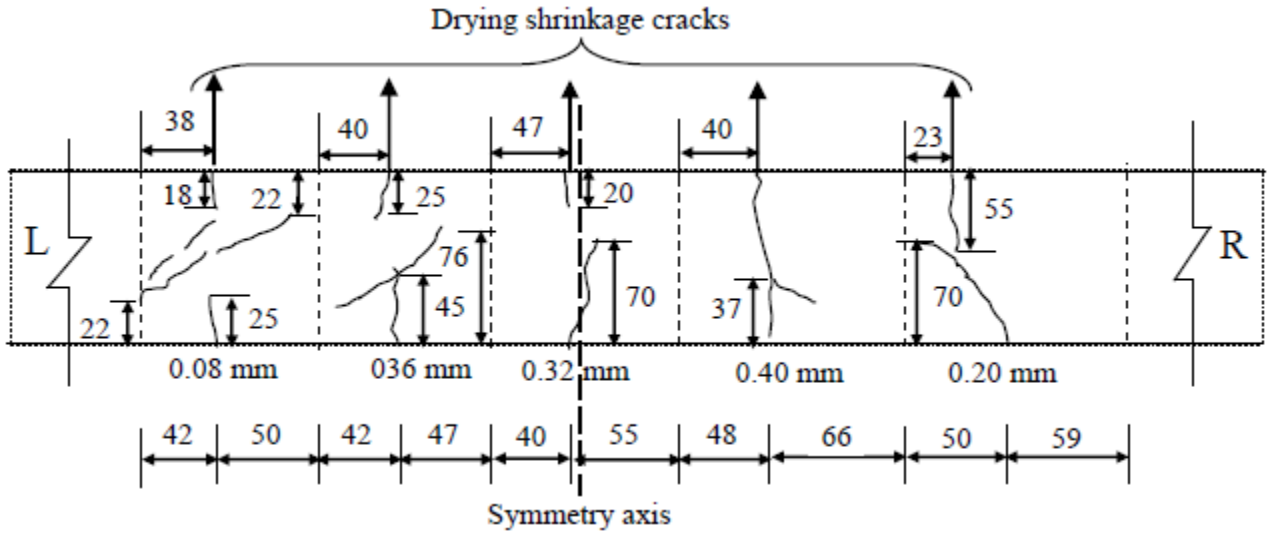
Drying shrinkage cracks
38
40
47
40
23
18
22
25
20
55
L
R
76
45
70
37
70
22
25
0.08 mm
036 mm
0.32 mm
0.40 mm
0.20 mm
42
50
42
47
40
55
48
66
50
59
Symmetry axis

(a)

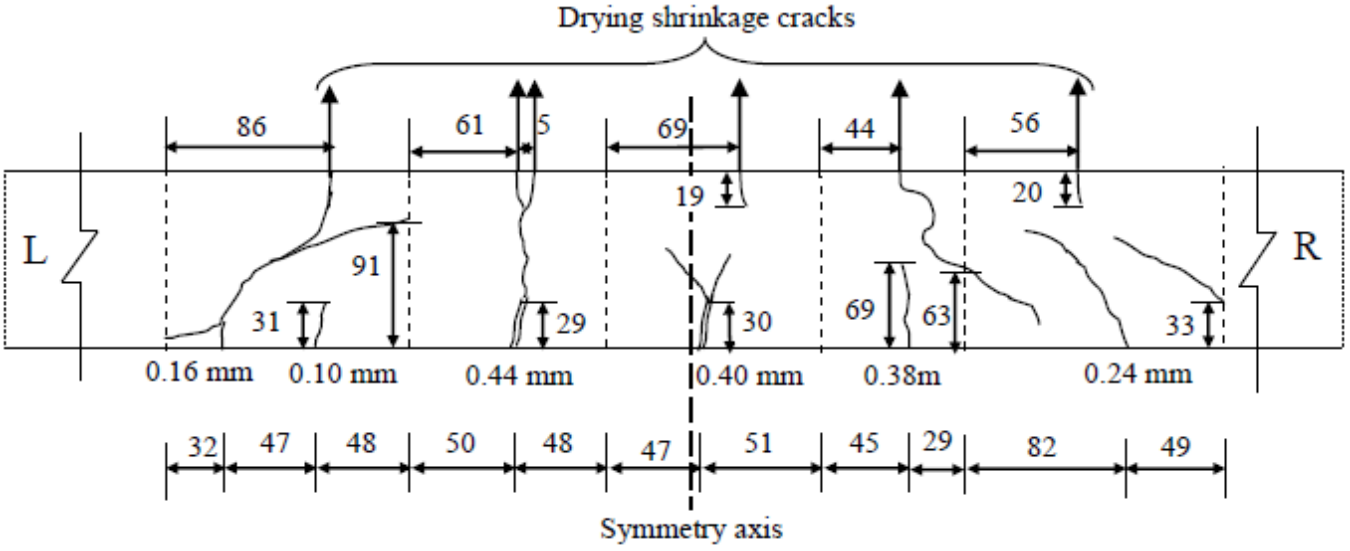
Drying shrinkage cracks
86
61
5
69
44
56
19
20
L
R
91
31
29
30
69
63
33
0.16 mm
0.10 mm
0.44 mm
0.40 mm
0.38m
0.24 mm
32
47
48
50
48
47
51
45
29
82
49
Symmetry axis

(b)

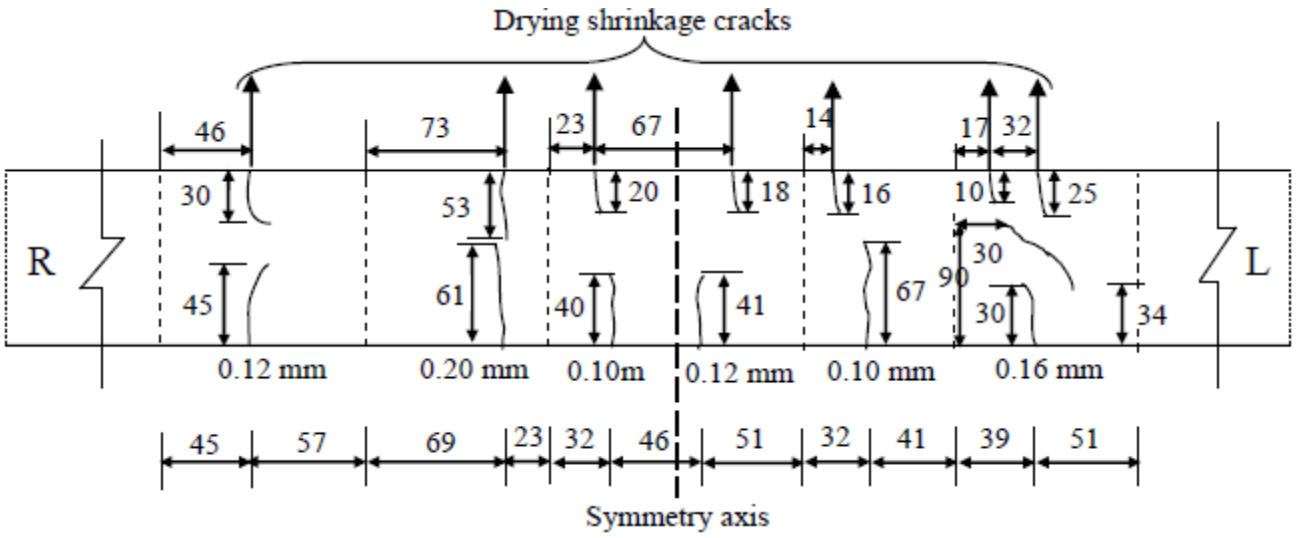

(c)

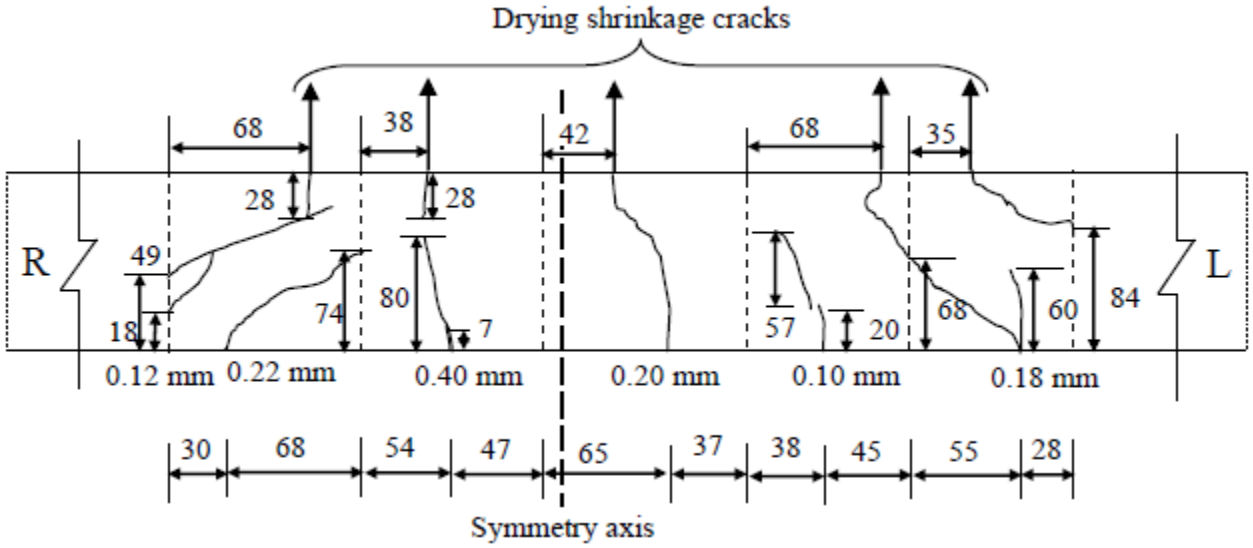

(d)

Figure 7. Crack patterns on lateral surfaces of the beam specimens made from FA concretes: (a) 040FA01; (b) 040FA03(2); (c) 055FA01; (d) 055FA03.

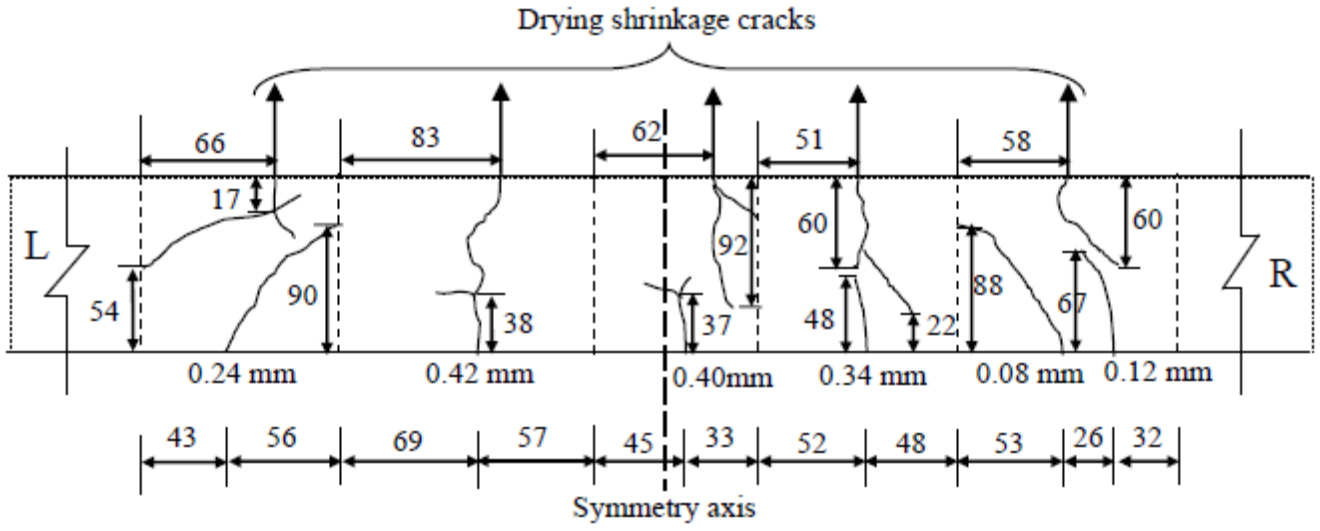

(a)

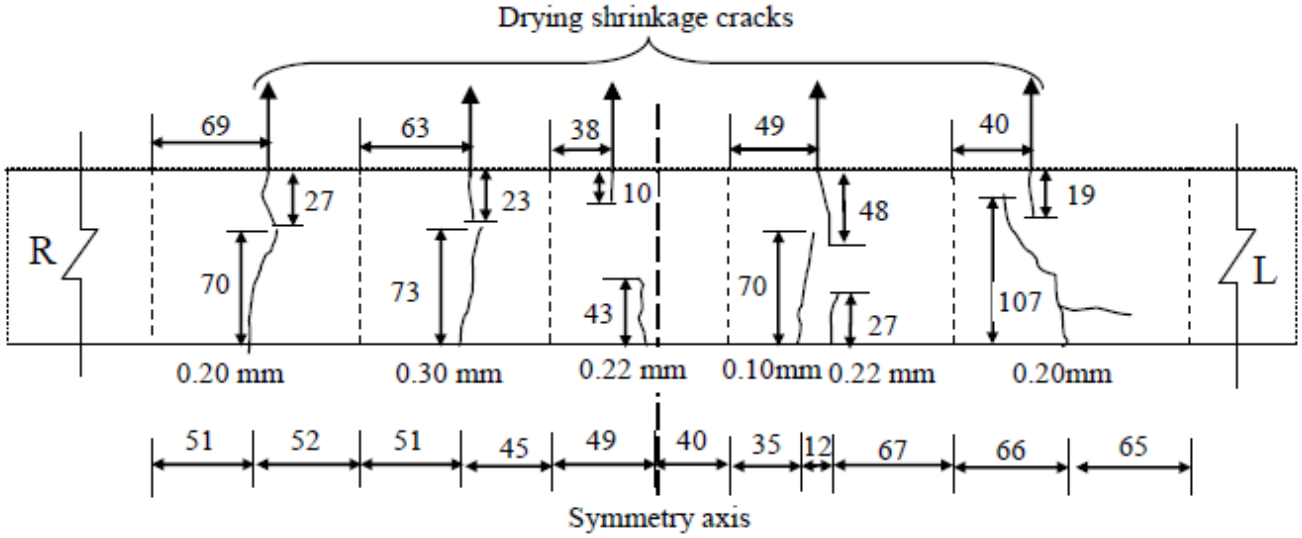

(b)

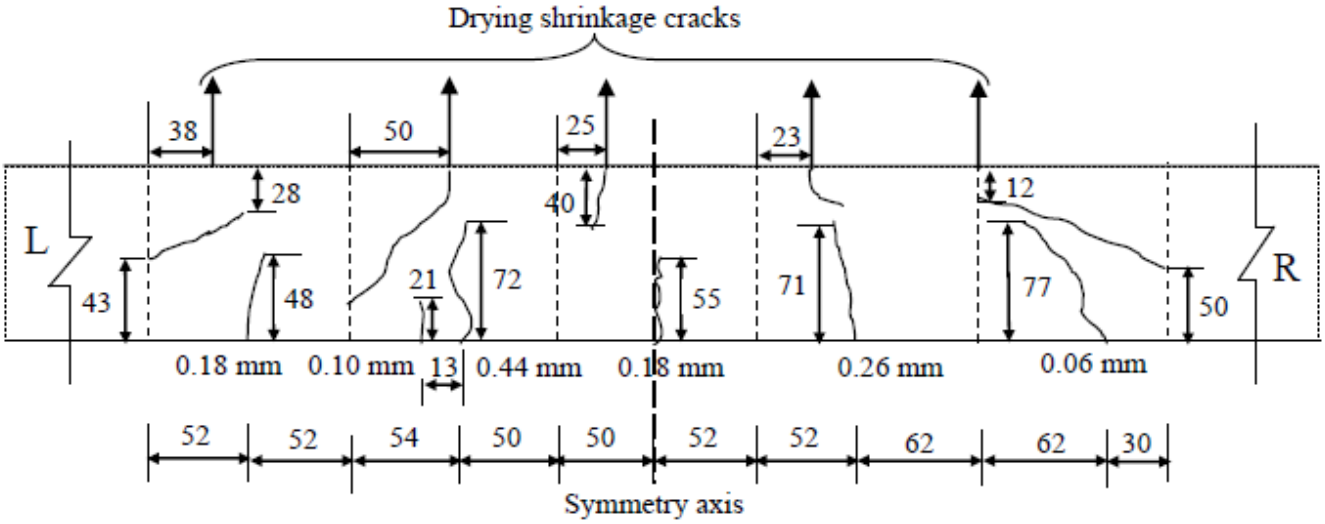

(c)

Figure 8. Crack patterns on lateral surfaces of the beam specimens made from GGBS concretes: (a) 040GGBS03; (b) 055GGBS01; (d) 055GGBS03.

Figure 9. Carbonation profile in a 055PC cube.

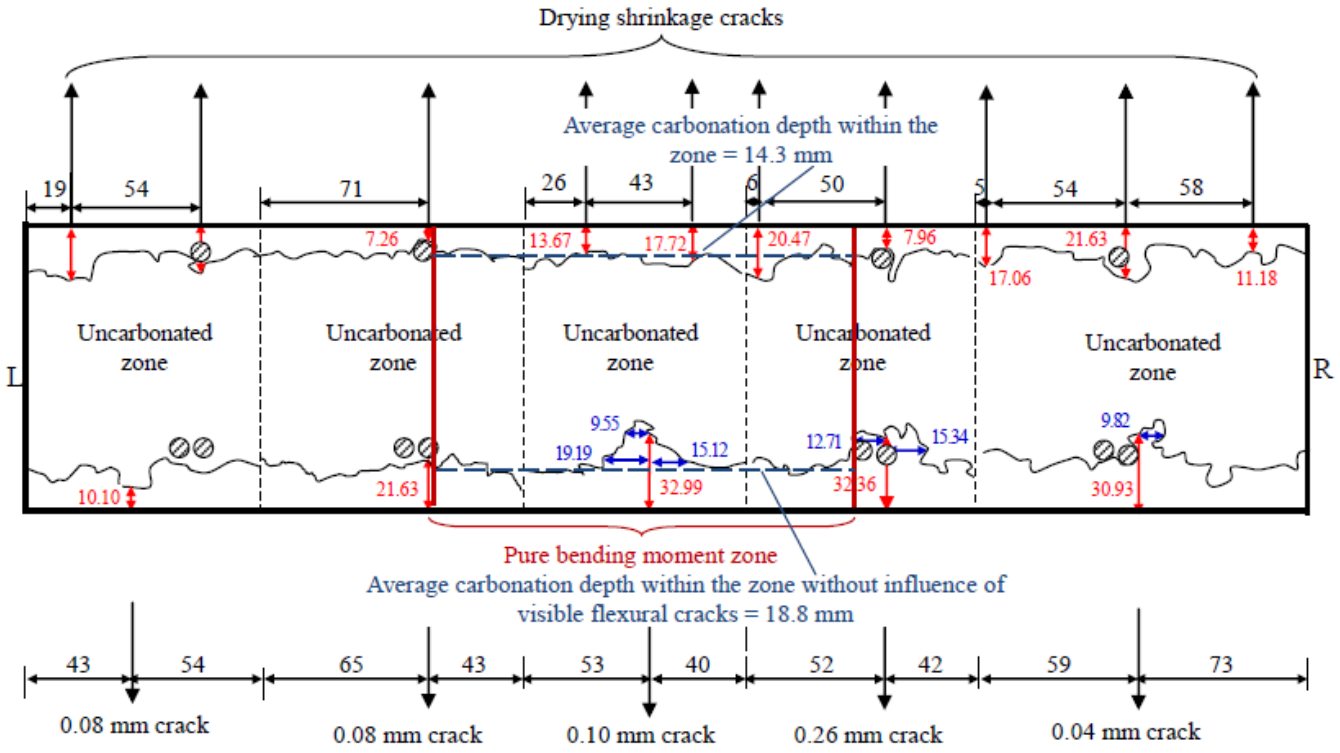

(a)

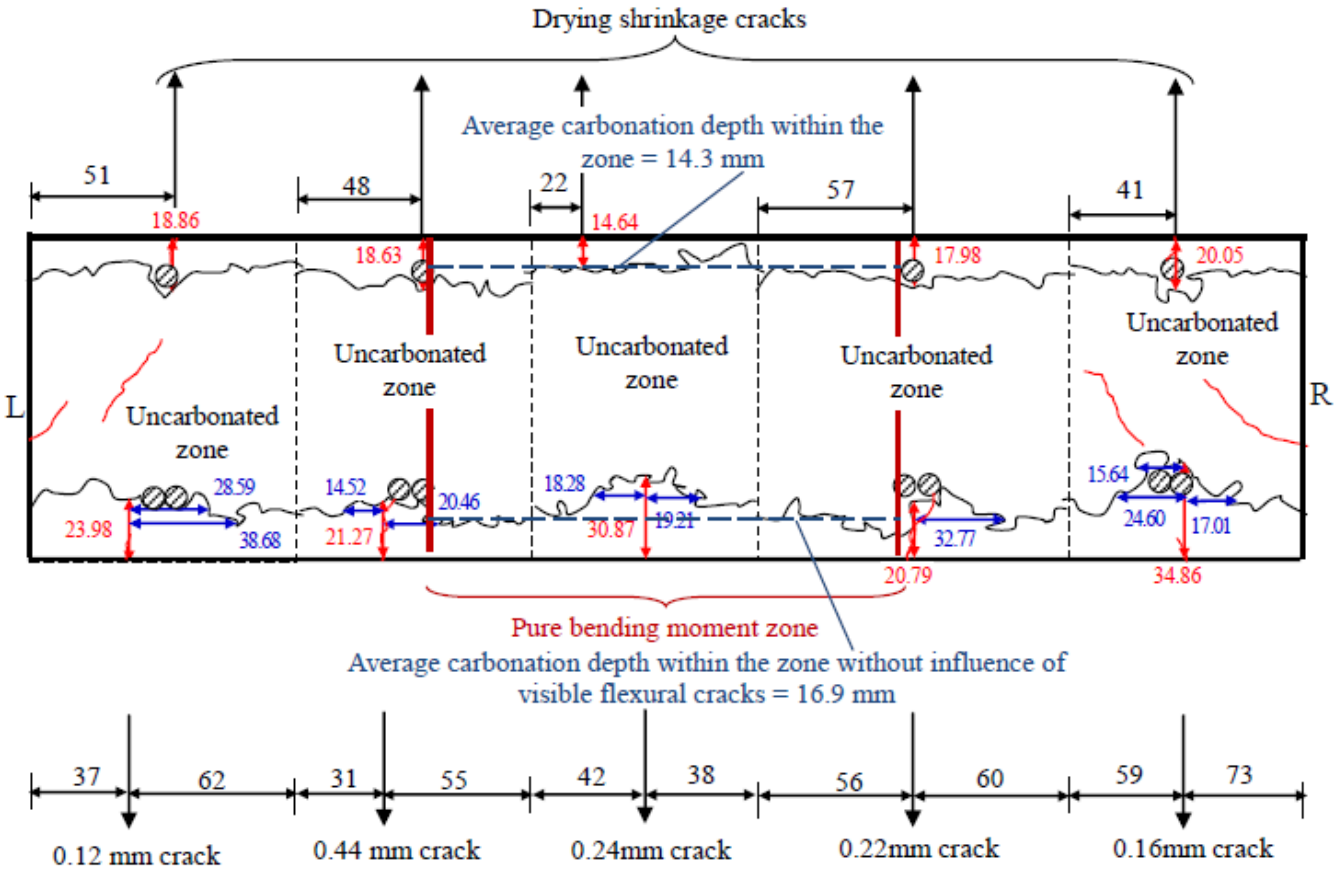

(b)

Figure 10. Carbonation profiles at the middle width of the beam specimens made from 055PC concrete: (a) 055PC01; (b) 055PC03.

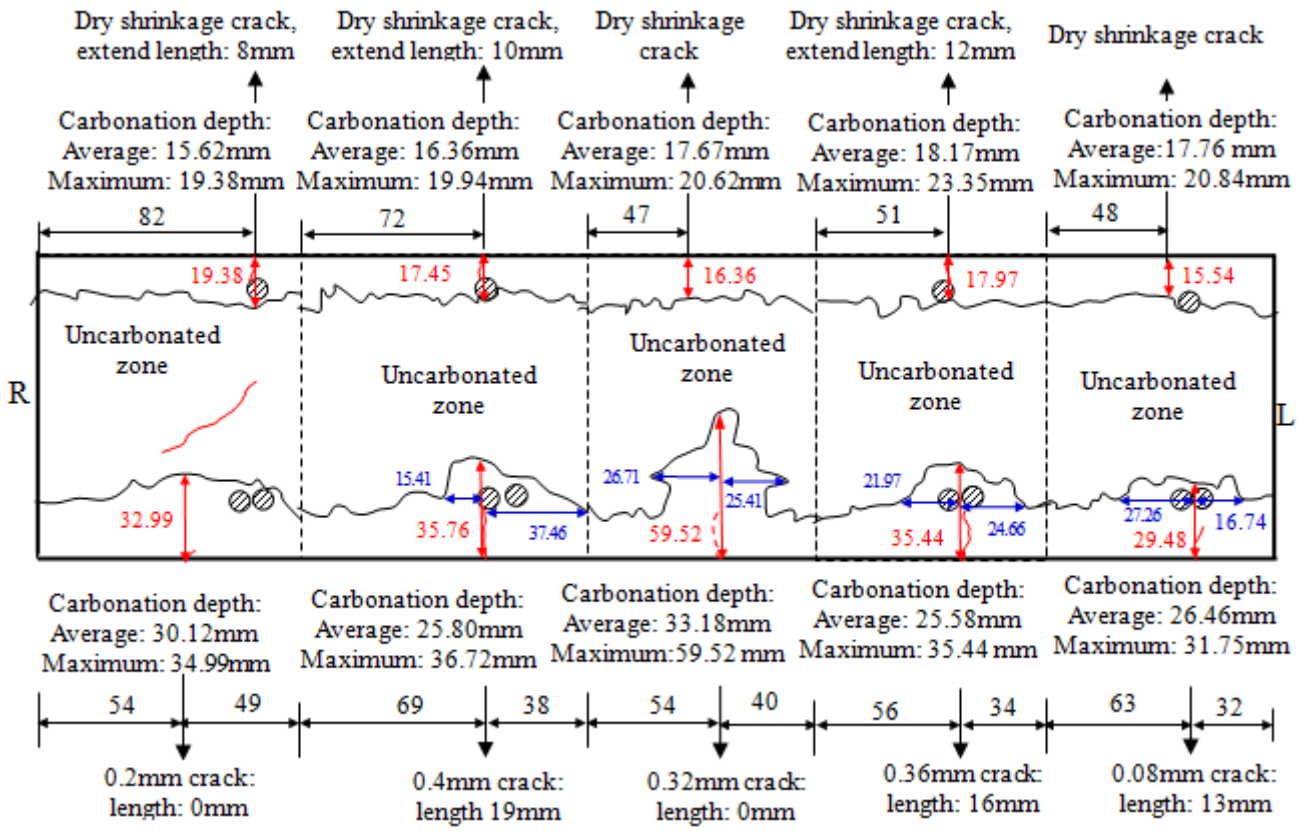
Dry shrinkage crack, extend length: 8mm
Dry shrinkage crack, extend length: 10mm
Dry shrinkage crack
Dry shrinkage crack, extend length: 12mm
Dry shrinkage crack
Carbonation depth: Average: 15.62mm Maximum: 19.38mm
Carbonation depth: Average: 16.36mm Maximum: 19.94mm
Carbonation depth: Average: 17.67mm Maximum: 20.62mm
Carbonation depth: Average: 18.17mm Maximum: 23.35mm
Carbonation depth: Average:17.76 mm Maximum: 20.84mm
82
72
47
51
48
19.38
17.45
16.36
17.97
15.54
R
L
Uncarbonated zone
Uncarbonated zone
Uncarbonated zone
Uncarbonated zone
Uncarbonated zone
32.99
15.41
35.76
37.46
26.71
25.41
59.52
21.97
35.44
24.66
27.26
29.48
16.74
Carbonation depth: Average: 30.12mm Maximum: 34.99mm
Carbonation depth: Average: 25.80mm Maximum: 36.72mm
Carbonation depth: Average: 33.18mm Maximum:59.52 mm
Carbonation depth: Average: 25.58mm Maximum: 35.44 mm
Carbonation depth: Average: 26.46mm Maximum: 31.75mm
54
49
69
38
54
40
56
34
63
32
0.2mm crack: length: 0mm
0.4mm crack: length 19mm
0.32mm crack: length: 0mm
0.36mm crack: length: 16mm
0.08mm crack: length: 13mm

(a)

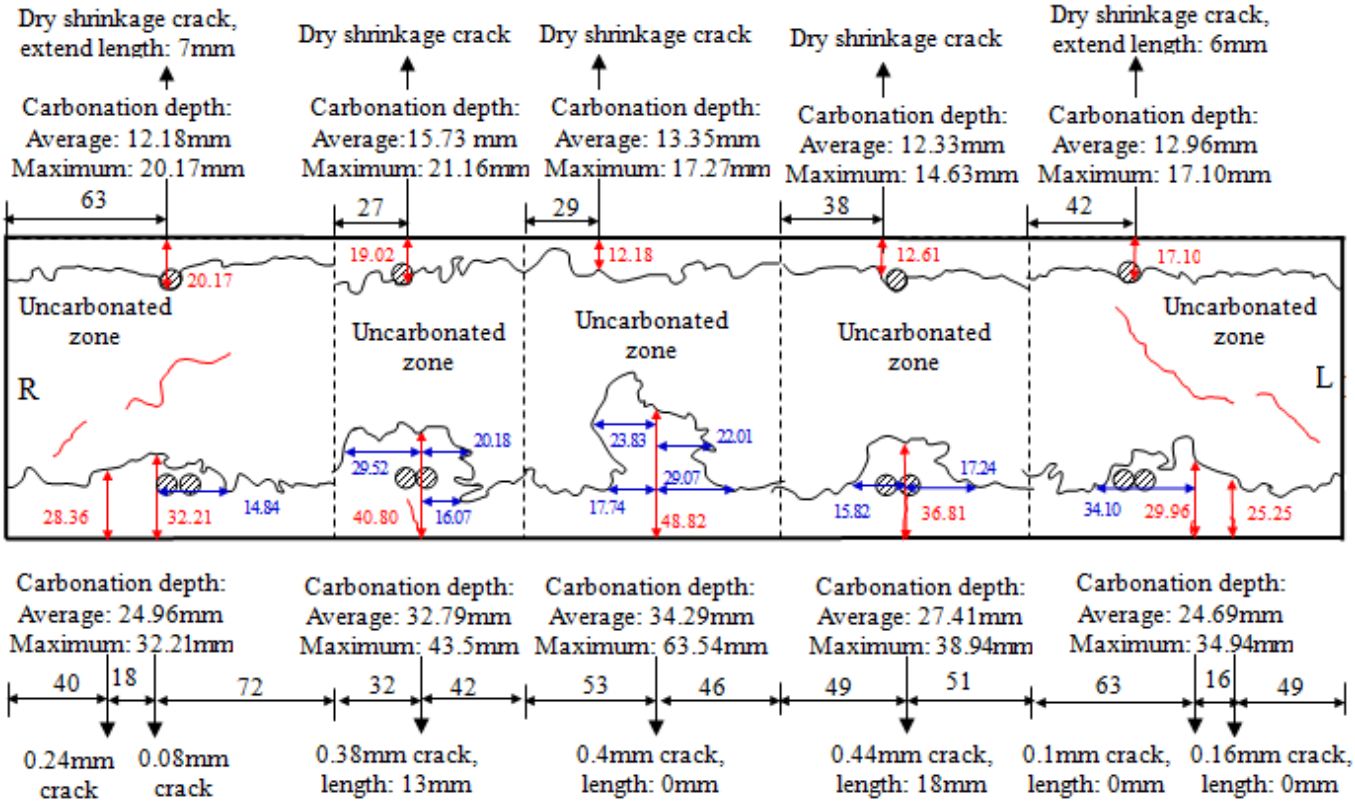
Dry shrinkage crack, extend length: 7mm
Dry shrinkage crack
Dry shrinkage crack
Dry shrinkage crack
Dry shrinkage crack, extend length: 6mm
Carbonation depth: Average: 12.18mm Maximum: 20.17mm
Carbonation depth: Average:15.73 mm Maximum: 21.16mm
Carbonation depth: Average: 13.35mm Maximum: 17.27mm
Carbonation depth: Average: 12.33mm Maximum: 14.63mm
Carbonation depth: Average: 12.96mm Maximum: 17.10mm
63
27
29
38
42
20.17
19.02
12.18
12.61
17.10
R
L
Uncarbonated zone
Uncarbonated zone
Uncarbonated zone
Uncarbonated zone
Uncarbonated zone
28.36
32.21
14.84
29.52
20.18
40.80
16.07
23.83
22.01
29.07
17.74
48.82
15.82
17.24
36.81
34.10
29.96
25.25
Carbonation depth: Average: 24.96mm Maximum: 32.21mm
Carbonation depth: Average: 32.79mm Maximum: 43.5mm
Carbonation depth: Average: 34.29mm Maximum: 63.54mm
Carbonation depth: Average: 27.41mm Maximum: 38.94mm
Carbonation depth: Average: 24.69mm Maximum: 34.94mm
40
18
72
32
42
53
46
49
51
63
16
49
0.24mm crack
0.08mm crack
0.38mm crack, length: 13mm
0.4mm crack, length: 0mm
0.44mm crack, length: 18mm
0.1mm crack, length: 0mm
0.16mm crack, length: 0mm

(b)

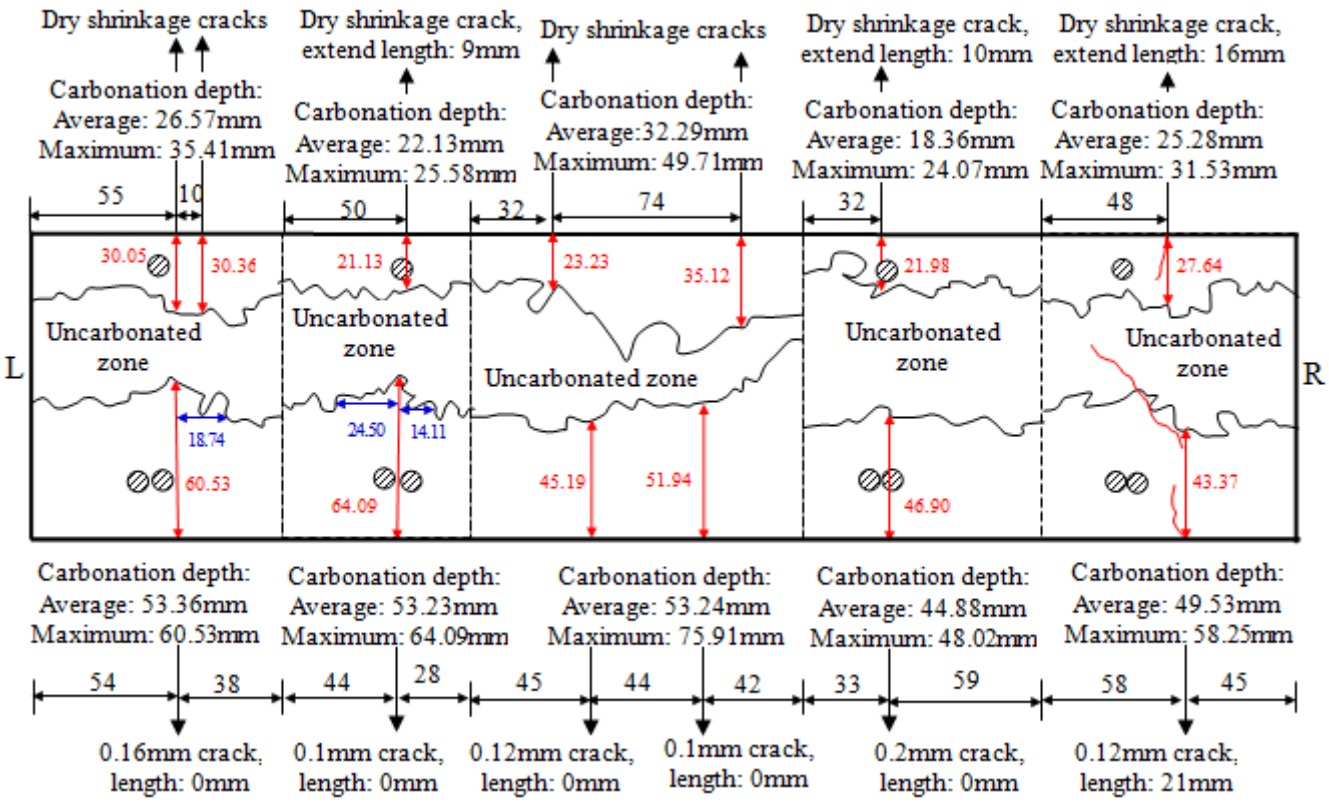

(c)

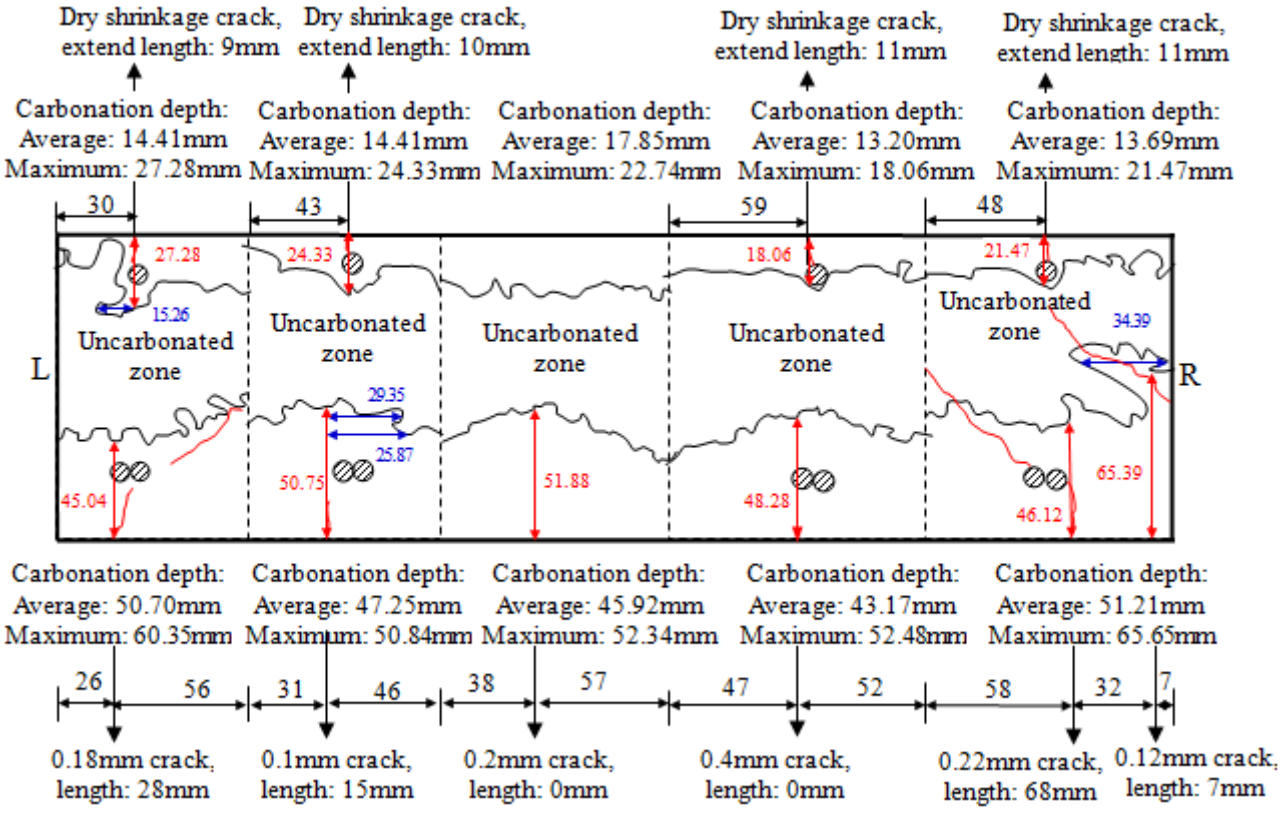

(d)

Figure 11. Carbonation profiles at the middle width of the beam specimens made from FA concretes: (a) 040FA01; (b) 040FA03(2); (c) 055FA01; (d) 055FA03.

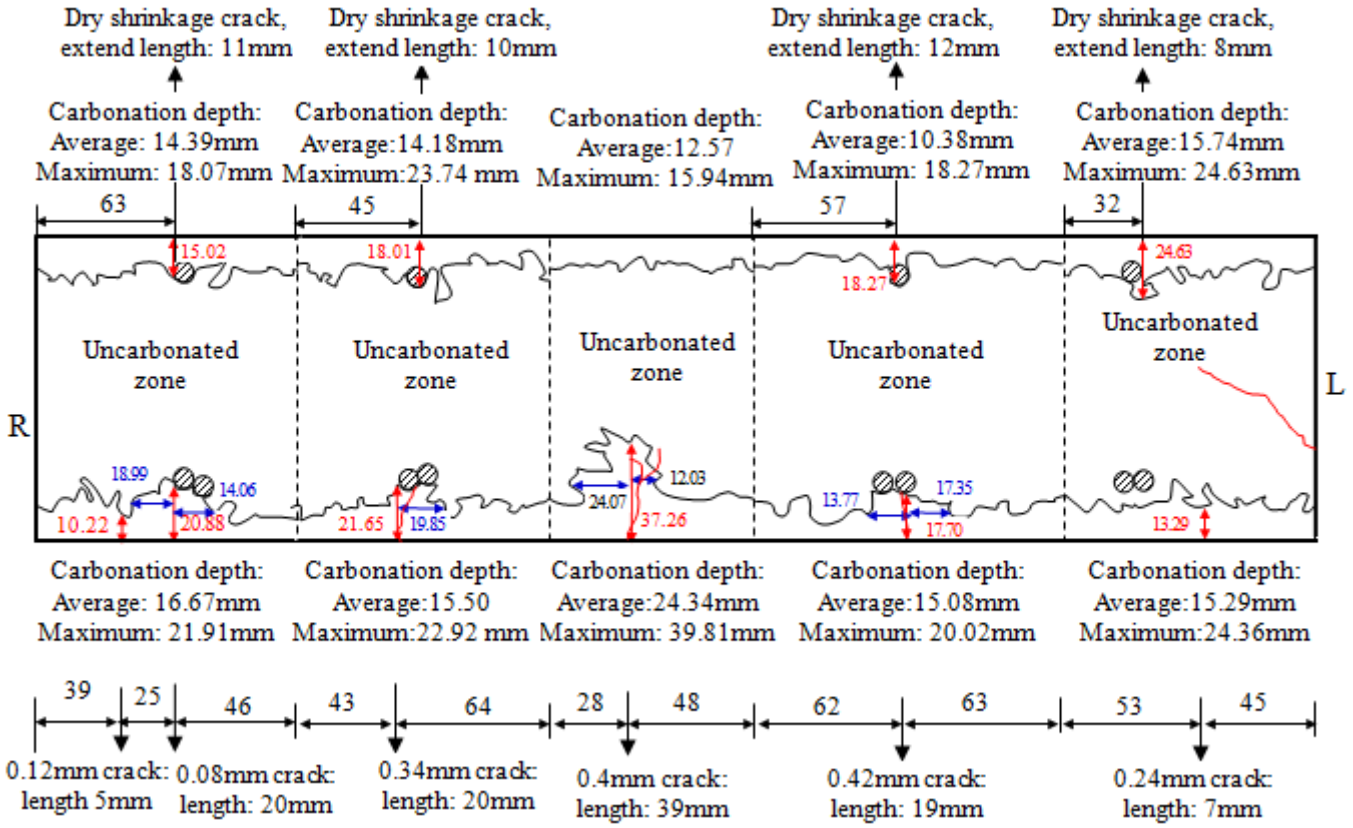
Dry shrinkage crack, extend length: 11mm
Dry shrinkage crack, extend length: 10mm
Dry shrinkage crack, extend length: 12mm
Dry shrinkage crack, extend length: 8mm
Carbonation depth: Average: 14.39mm Maximum: 18.07mm
Carbonation depth: Average:14.18mm Maximum:23.74 mm
Carbonation depth: Average:12.57 Maximum: 15.94mm
Carbonation depth: Average:10.38mm Maximum: 18.27mm
Carbonation depth: Average:15.74mm Maximum: 24.63mm
63
45
57
32
15.02
18.01
18.27
24.63
Uncarbonated zone
Uncarbonated zone
Uncarbonated zone
Uncarbonated zone
Uncarbonated zone
R
L
18.99
14.06
10.22
20.88
21.65
19.85
12.03
24.07
37.26
13.77
17.35
17.70
13.29
Carbonation depth: Average: 16.67mm Maximum: 21.91mm
Carbonation depth: Average:15.50 Maximum:22.92 mm
Carbonation depth: Average:24.34mm Maximum: 39.81mm
Carbonation depth: Average:15.08mm Maximum: 20.02mm
Carbonation depth: Average:15.29mm Maximum:24.36mm
39
25
46
43
64
28
48
62
63
53
45
0.12mm crack: length 5mm
0.08mm crack: length: 20mm
0.34mm crack: length: 20mm
0.4mm crack: length: 39mm
0.42mm crack: length: 19mm
0.24mm crack: length: 7mm

(a)

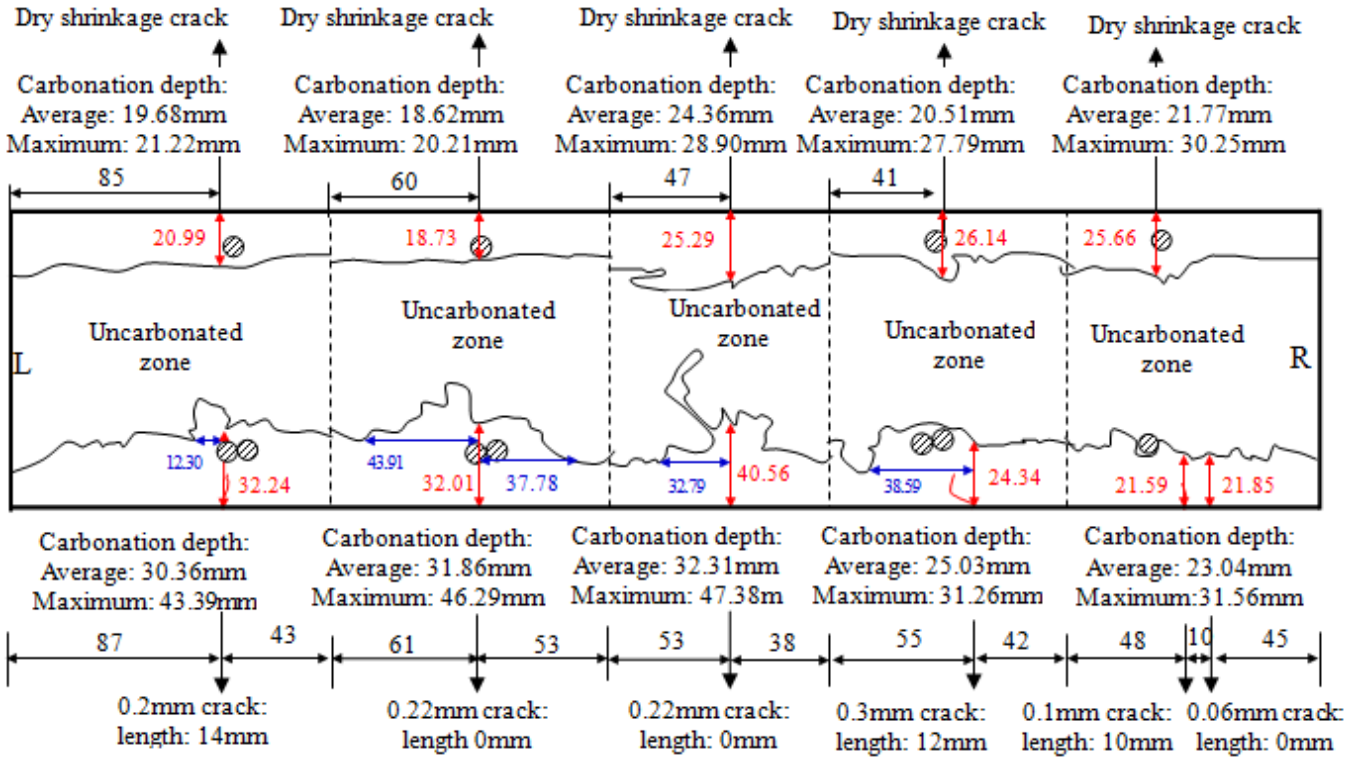
Dry shrinkage crack
Dry shrinkage crack
Dry shrinkage crack
Dry shrinkage crack
Dry shrinkage crack
Carbonation depth: Average: 19.68mm Maximum: 21.22mm
Carbonation depth: Average: 18.62mm Maximum: 20.21mm
Carbonation depth: Average: 24.36mm Maximum: 28.90mm
Carbonation depth: Average: 20.51mm Maximum:27.79mm
Carbonation depth: Average: 21.77mm Maximum: 30.25mm
85
60
47
41
20.99
18.73
25.29
26.14
25.66
Uncarbonated zone
Uncarbonated zone
Uncarbonated zone
Uncarbonated zone
Uncarbonated zone
L
R
12.30
32.24
43.91
32.01
37.78
32.79
40.56
38.59
24.34
21.59
21.85
Carbonation depth: Average: 30.36mm Maximum: 43.39mm
Carbonation depth: Average: 31.86mm Maximum: 46.29mm
Carbonation depth: Average: 32.31mm Maximum: 47.38m
Carbonation depth: Average: 25.03mm Maximum: 31.26mm
Carbonation depth: Average: 23.04mm Maximum:31.56mm
87
43
61
53
53
38
55
42
48
10
45
0.2mm crack: length: 14mm
0.22mm crack: length 0mm
0.22mm crack: length: 0mm
0.3mm crack: length: 12mm
0.1mm crack: length: 10mm
0.06mm crack: length: 0mm

(b)

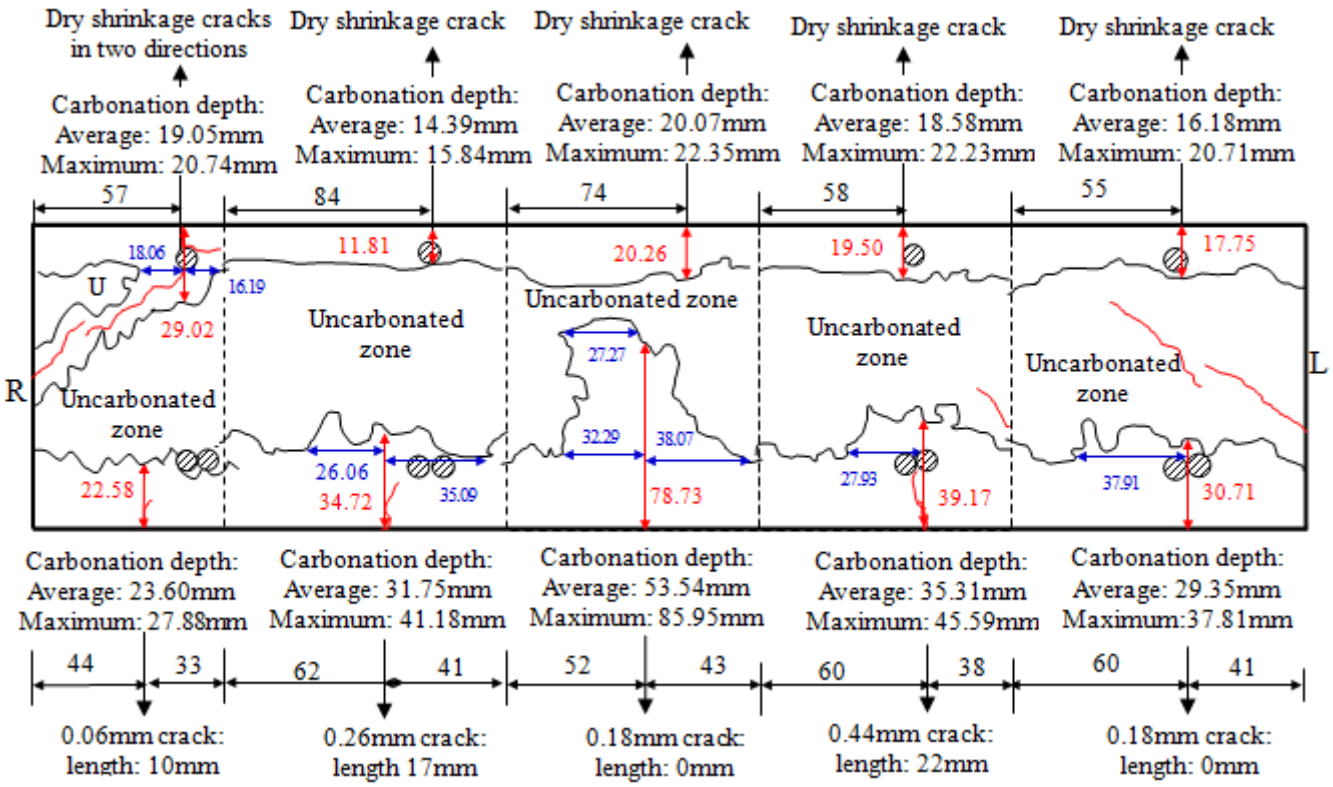

(c)

Figure 12. Carbonation profiles at the middle width of the beam specimens made from GGBS concretes: (a) 040GGBS03; (b) 055GGBS01; (c) 055GGBS03.

Tables

Table 1 Mix constituent proportions of concretes (kg/m^3)

Concrete mix	Water	Portland Cement (CEM I 52.5 N)	SCM	Sand	10-mm gravel	Plasticizer	w/b ratio
040PC	148	370	0	765	1120	19	0.40
055PC	200	360	0	740	1110	–	0.55
040FA	148	260	FA: 110	765	1130	9.5	0.40
055FA	194	250	FA: 107	740	1110	–	0.54
040GGBS	145	180	GGBS: 180	755	1135	12	0.40
055GGBS	200	182	GGBS: 182	740	1110	–	0.55

Table 2 Details of RC beam specimens

Test specimens	Cross section (mm)		Average clear concrete cover of 10-mm bars in tensile zone (mm)	Average clear concrete cover of stirrups		Maximum width of flexural cracks (mm)	Concrete compressive strength (MPa)
	Width	Height		Tensile zone	Compression zone		
040PC01	100.2	119.7	29.1	21.0	9.8	0.20	72.9
040PC03	99.6	121.9	28.4	19.5	11.5	0.64	
055PC01	99.4	120.5	29.9	22.7	8.9	0.26	47.9
055PC03	99.5	121.3	30.5	22.7	8.5	0.44	
040FA01	100.4	121.0	28.7	19.3	10.6	0.40	58.9
040FA03	98.8	120.5	27.5	19.2	13.3	0.40	
040FA03(2)	98.8	120.6	27.9	18.1	11.1	0.44	
055FA01	99.4	120.1	27.4	18.3	9.9	0.20	45.3
055FA03	98.6	120.6	30.0	22.1	10.3	0.40	
040GGBS03	98.9	121.2	29.2	20.1	9.1	0.42	67.6
055GGBS01	99.1	120.9	28.9	21	9.5	0.30	54.9
055GGBS03	100.5	121.2	28.1	19.5	9.5	0.44	

Table 3 Absorption and void content of concretes

Concrete mix	Concrete cubes											
		Mass in air (g)			Mass in water* (g)	Volume (cm^3)	Density (kg/m3)			Absorption	Void content	
		As-received	Oven-dried	Water saturated			As-received	Oven-dried	Water saturated	(%)	(%)	Mean
040PC	1	2378.6	2317.4	2440.7	1379.8	994.3	2392.2	2330.7	2455.7	5.3	12.4	12.3
	2	2403.7	2343.1	2465.5	1396.6	1002.3	2398.2	2337.7	2459.8	5.2	12.2	
055PC	1	2288.2	2231.3	2383.6	1322.9	994.1	2301.8	2244.5	2397.7	6.8	15.3	15.2
	2	2301.2	2243.2	2393.5	1332.3	994.6	2313.7	2255.4	2406.5	6.7	15.1	
040FA	1	2352.7	2299.2	2430.7	1355.2	1008.9	2331.9	2278.9	2409.3	5.7	13.0	12.9
	2	2358.5	2308.5	2437.5	1362.6	1008.3	2339.1	2289.5	2417.4	5.6	12.8	
055FA	1	2298.3	2246.1	2402.0	1330.4	1005.0	2286.9	2234.9	2390.0	6.9	15.5	15.6
	2	2291.6	2238.2	2394.6	1325.2	1002.8	2285.2	2232.0	2387.9	7.0	15.6	
040GGBS	1	2403.2	2336.8	2458.9	1385.4	1006.9	2386.7	2320.8	2442.0	5.2	12.1	12.1
	2	2418.3	2351.9	2473.5	1393.2	1013.7	2385.6	2320.1	2440.1	5.2	12.0	
055GGBS	1	2347.6	2284.1	2429.8	1355.7	1007.5	2330.1	2267.1	2411.7	6.4	14.5	14.5
	2	2351.0	2281.8	2427.9	1353.5	1007.8	2332.8	2264.1	2409.1	6.4	14.5	

*The mass includes the mass of the stirrup (66.6 g) that supported the immersed concrete cube in water

Table 4 Carbonation depths in specimens

Concrete type	Specimens		Average carbonation depth* (mm)		Maximum carbonation depth (mm)	
			Top	Bottom	Top	Bottom
040PC	Cube		0	0	-	-
	Beams	040PC01	0	0	0	0
		040PC03	3.5	6.3	17.2	17.8
055PC	Cube		18.9	16.1	-	-
	Beams	055PC01	14.3	18.8	25.5	43.5
		055PC03	14.3	16.9	24.7	38.9
040FA	Cube		19.3	18.5	-	-
	Beams	040FA01	17.0	20.8	23.3	59.7
		040FA03	17.9	24.4	30.6	52.0
		040FA03(2)	13.5	19.6	20.6	63.6
055FA	Cube		24.4	18.5	-	-
	Beams	055FA01	25.4	48.1	49.7	64.1
		055FA03	16.1	38.8	28.7	65.7
040GGBS	Cube		11.6	10.6	-	-
	Beam	040GGBS03	10.6	15.1	24.6	42.9
055GGBS	Cube		15.2	12.0	-	-
	Beams	055GGBS01	21.6	24.4	30.2	47.4
		055GGBS03	19.0	29.8	23.7	86.0

* Over the 200-mm long central segment excluding the influence of visible flexural cracks